NASA/TM–20250008644

# A Preliminary Assessment of Thermoplastic Composite Welding for In-Space Applications by the Thermoplastics Development for Exploration Applications (TDEA) Project

*Andrew C. Bergan[1], Sandi G. Miller[2], Kenneth N. Segal[3,4], William D. Mulhearn[3], Allison M. Clark[5], Marc R. Schultz[1], Joseph J. Pinakidis[2], Babak Farrokh[3], John Chiu[3,6], Ronald L. Glenn[3], Arunkumar Satyanarayana[1], Richard W. Rauser[2,7], Patrick H. Johnston[1], Joshua M. Fody[1], Ji Su[1], and Frank A. Leone[1]*

[1]*Langley Research Center, Hampton, Virginia*
[2]*Glenn Research Center, Cleveland, Ohio*
[3]*Goddard Space Flight Center, Greenbelt, Maryland*
[4]*Intuitive Machines, Incorporated, Greenbelt, Maryland*
[5]*Marshall Space Flight Center, Huntsville, Alabama*
[6]*Actalent Corporation, Greenbelt, Maryland*
[7]*University of Toledo, Toledo, Ohio*

September 2025

## NASA STI Program Report Series

Since its founding, NASA has been dedicated to the advancement of aeronautics and space science. The NASA scientific and technical information (STI) program plays a key part in helping NASA maintain this important role.

The NASA STI program operates under the auspices of the Agency Chief Information Officer. It collects, organizes, provides for archiving, and disseminates NASA's STI. The NASA STI program provides access to the NTRS Registered and its public interface, the NASA Technical Reports Server, thus providing one of the largest collections of aeronautical and space science STI in the world. Results are published in both non-NASA channels and by NASA in the NASA STI Report Series, which includes the following report types:

- TECHNICAL PUBLICATION. Reports of completed research or a major significant phase of research that present the results of NASA Programs and include extensive data or theoretical analysis. Includes compilations of significant scientific and technical data and information deemed to be of continuing reference value. NASA counterpart of peer-reviewed formal professional papers but has less stringent limitations on manuscript length and extent of graphic presentations.

- TECHNICAL MEMORANDUM. Scientific and technical findings that are preliminary or of specialized interest, e.g., quick release reports, working papers, and bibliographies that contain minimal annotation. Does not contain extensive analysis.

- CONTRACTOR REPORT. Scientific and technical findings by NASA-sponsored contractors and grantees.

- CONFERENCE PUBLICATION. Collected papers from scientific and technical conferences, symposia, seminars, or other meetings sponsored or co-sponsored by NASA.

- SPECIAL PUBLICATION. Scientific, technical, or historical information from NASA programs, projects, and missions, often concerned with subjects having substantial public interest.

- TECHNICAL TRANSLATION. English-language translations of foreign scientific and technical material pertinent to NASA's mission.

Specialized services also include organizing and publishing research results, distributing specialized research announcements and feeds, providing information desk and personal search support, and enabling data exchange services.

For more information about the NASA STI program, see the following:

- Access the NASA STI program home page at http://www.sti.nasa.gov

- Help desk contact information:

https://www.sti.nasa.gov/sti-contact-form/
and select the "General" help request type.

NASA/TM–20250008644

# A Preliminary Assessment of Thermoplastic Composite Welding for In-Space Applications by the Thermoplastics Development for Exploration Applications (TDEA) Project

*Andrew C. Bergan[1], Sandi G. Miller[2], Kenneth N. Segal[3,4], William D. Mulhearn[3], Allison M. Clark[5], Marc R. Schultz[1], Joseph J. Pinakidis[2], Babak Farrokh[3], John Chiu[3,6], Ronald L. Glenn[3], Arunkumar Satyanarayana[1], Richard W. Rauser[2,7], Patrick H. Johnston[1], Joshua M. Fody[1], Ji Su[1], and Frank A. Leone[1]*

[1]*Langley Research Center, Hampton, Virginia*
[2]*Glenn Research Center, Cleveland, Ohio*
[3]*Goddard Space Flight Center, Greenbelt, Maryland*
[4]*Intuitive Machines, Incorporated, Greenbelt, Maryland*
[5]*Marshall Space Flight Center, Huntsville, Alabama*
[6]*Actalent Corporation, Greenbelt, Maryland*
[7]*University of Toledo, Toledo, Ohio*

National Aeronautics and
Space Administration

Langley Research Center
Hampton, Virginia 23681-2199

September 2025

Available from:

NASA STI Program / Mail Stop 050
NASA Langley Research Center
Hampton, VA 23681-2199

## Acknowledgements

We gratefully acknowledge the partnerships with the National Institute for Aviation Research (NIAR), Spirit AeroSystems, and Agile Ultrasonics that made this work possible. Specifically, the contributions from Mark Walthers, Shakya Liyanage, and the manufacturing and test team at NIAR; Samuel Slater and Mark Wadsworth at Spirit; and John Hertel, Chris Skocik, Matt Short, and Jim Stratton at Agile were invaluable. Thank you to the team at Mantis Composites for supplying the additively manufactured adherends used in welding trials. We thank Charles He for making the coefficient of thermal expansion measurements. We are also in debt to David Myers, Daniel Drake, W. Thomas Haynie, Michael McNeill, Nate Gardner, David Dawicke, George Cowley, Wyatt Healy, Andrew Glendening, William Sommer, and Johnny Callahan for their contributions to the subelement tests. Finally, we also appreciate Chris Wohl, Valerie Wiesner, and Brandon Widener for sharing their design and experience with a lunar regolith simulant application apparatus, which was the basis for the system used in this work.

# Abstract

Thermoplastic composite (TPC) welding shows promise for future in-space structural joining applications. NASA's Thermoplastics Development for Exploration Applications (TDEA) project contributed to this long-term objective through hundreds of welding trials and evaluations on various joint configurations. This report summarizes the key findings from these welding trials and assesses the potential for in-space applications of this technology. The welding trials include coupon-scale assessments of resistance, induction, and ultrasonic welding methods in a lab environment. The weld methods are applied to five TPC materials including amorphous and semicrystalline resins. A single lap-shear configuration is used with welds conducted on individual specimens (i.e., spot welds) relevant for assembling truss structures. Defects, such as unwelded regions, delamination, porosity, or distortion (thinning, fiber pushout) occurred for all weld methods and material combinations. Defects were detected by nondestructive evaluation (NDE) and verified by optical microscopy. Despite the defects, high lap-shear strength (LSS) and low coefficient of variation (COV) were achieved for some combinations of weld method and material system. In general, the extent of defects was lower and the LSS was higher when the welding organization had substantial previous experience with the material system. This highlights the sensitivity of this technology to weld processing parameters and the need for extensive process development. Based on the coupon-scale welding experience, the welding method advantages, limitations, and technology gaps are summarized. For the three weld methods, accurately controlling the pressure and temperature during welding is essential to produce a strong, well-consolidated weld. However, desirable pressure and temperature histories can be difficult to obtain since they are not controlled directly during the welding processes examined herein. Welded joints between adherends that have different resin systems or made with different manufacturing processes using similar resin systems are also assessed and show potential for a variety of applications.

A specific application was chosen by the TDEA project as a test case to evaluate manufacturing scale-up. The application is for a 168-ft-tall truss tower to be located at the lunar south pole and constructed with welded joints on the lunar surface. A subelement-scale structural joint representing the most highly loaded joint was manufactured and tested. Ultrasonic welding was selected for this application. In preparation for the subelement fabrication, scale-up welding trials were also conducted. Two ultrasonic joining processes were successfully developed and tested to loads exceeding the design requirement. All manufacturing was completed in a lab environment. To help address the applicability of this technology for in-space applications, material properties of specific interest for space environments such as outgassing and coefficient of thermal expansion (CTE) are reported. Ultrasonic welding trials with lunar regolith contamination were conducted and show low sensitivity to contamination. This low sensitivity is important for welding on dusty planetary bodies. Finally, a summary is provided of a preliminary study showing the feasibility of weld reassembly at the coupon scale to allow for repair or reconfiguration to meet future mission needs. Overall, the results show that strong welds that meet design requirements are possible, and is demonstrated at the coupon and subelement scale. Substantial process development effort is required to obtain this outcome for a particular weld method, material, and welding configuration and to control joint strength variability. Future work is needed to develop a better understanding of the weld processes, adapt them to space environments through trials in thermal vacuum chambers, and characterize the structural behavior of the welded joints under relevant environments.

# List of Acronyms

| | |
|---|---|
| AM | Additive manufacturing |
| AFP | Automated fiber placement |
| COV | Coefficient of variation |
| CTE | Coefficient of thermal expansion |
| CVCM | Collected volatile condensable materials |
| DCB | Double cantilever beam |
| DCDT | Direct current displacement transformer |
| DIC | Digital image correlation |
| DLL | Design limit load |
| DLS | Double lap shear |
| ED | Energy director |
| FE | Finite element |
| GPR | Gaussian process regression |
| HAZ | Heat affected zone |
| ICAT | In-situ consolidated AFP of thermoplastics |
| JSP | Joint splice plate |
| LEO | Low earth orbit |
| LM-PAEK | Low-melt polyaryletherketone |
| LSS | Lap shear strength |
| MSFC | Marshall Space Flight Center |
| NCAMP | National Center for Advanced Materials Performance |
| NDE | Nondestructive evaluation |
| NIAR | National Institute for Aviation Research |
| PEEK | Polyetheretherketone |
| PEI | Polyetherimide |
| PEKK | Polyetherketoneketone |
| PPS | Polyphenylene sulfide |
| QI | Quasi-isotropic |
| SLS | Single lap shear |
| SMAP | Soil Moisture Active/Passive |
| TDEA | Thermoplastics Development for Exploration Applications |
| TML | Total mass loss |
| TPC | Thermoplastic composite |
| TRL | Technology readiness level |
| TSC | Thermoset composite |
| TSPD | Thermoplastic in-space point design |
| VTE | Vertical truss element |
| WVR | Water vapor regained |
| XRCT | X-ray computed tomography |

# 1 Introduction

The concept of in-space manufacturing operations using thermoplastic composite (TPC) materials to produce huge space structures is a longstanding vision pursued intermittently since at least the 1970s [1, 2]. The appeal of this concept is rooted in relatively simple manufacturing processes using temperature and pressure (e.g., pultrusion) that can transform lightweight thermoplastic composite feedstock into stiff structural elements. In recent years, NASA initiated efforts to develop flight demonstrations of in-space neat thermoplastic and thermoplastic composite structure manufacturing, but subsequently canceled the programs due schedule, budget overruns, or technical challenges [3, 4]. Although manufacturing structural elements in-space may be possible someday, in-space assembly of terrestrially manufactured structural elements is likely more easily achieved. In-space joining can also be applied to assemble large trusses [5], thereby enabling very large reflectors and arrays without the complexity of deployables. The same technology also has the potential to construct and assemble surface infrastructure such as towers and trusses on the planetary surfaces of the Moon and Mars [6, 7].

Developments of technology for structural in-space assembly of trusses have often been pursued with thermoset composite (TSC) tubes having bonded metallic end fittings that were preassembled terrestrially, e.g. [8]. These structural elements can then assembled in-space with welding or mechanical fasteners used at the joints [8, 9]. Instead, if the truss elements were manufactured from TPCs, the elements themselves can be welded together, to eliminate the need for adhesive bonding, metallic end fittings, or fasteners. Therefore, TPC welding in-space offers the potential to reduce part count and mass. An all-TPC joint may also offer benefits from a thermostructural perspective in that coefficient of thermal expansion (CTE) mismatch is limited to the fiber-matrix interface.

Other material systems have been considered for in-space structural joining. Vitrimers are a special class of thermoset materials that have reversible bonding capability through pressure and temperature application (similar to TPC welding), and are being pursued by others for in-space assembly applications [10]. Besides welding and mechanical fastening, chemical bonding is the other category of structural joining that is commonly used. However, chemical bonding does not appear suitable for in-space application due to the stringent surface preparation requirements and offgassing from the chemical reaction.

TPC welding can be applicable to a large variety of structural applications and mission needs. TPC welding provides a pathway toward larger-scale in-space manufacturing since the underlying physics of the welding and manufacturing processes are similar. A fully consolidated weld resembles the laminate condition after autoclave processing with full crystallization, low porosity, and high polymer chain entanglement across the weld interface. The polymer should be indiscernible from the interlaminar interfaces away from the weld. In addition to pultrusion, in-situ consolidated automated fiber placement of thermoplastics (ICAT) is also a candidate for future in-space manufacturing. In ICAT, TPC tows are essentially laser welded in place to build up the structure one layer at a time. TPC welding is also a good candidate for joining additively manufactured (AM) secondary structures (which commonly use thermoplastic materials) to larger structures.

NASA established the Thermoplastics Development for Exploration Applications (TDEA) project to advance TPC joining technology for future exploration mission needs. TDEA conducted manufacturing trials, tests, and evaluation of three thermoplastic composite (TPC) welding methods: resistance, induction, and ultrasonic. The primary difference among the three welding methods is the heat generation method, as shown in Figure 1. Resistance welding generates heat at the substrate interface by passing current through a resistive heating element. Induction welding uses a coil to generate a magnetic field, which induces eddy currents in the carbon fibers of the substrates, which generate heat. Ultrasonic welding applies high-amplitude ultrasonic waves to the substrates which leads to frictional heating (surface and viscoelastic). TDEA also pursued scale-up of ultrasonic welding for application to assembly of a tower truss structure on the lunar surface. This application is referred to as the thermoplastic in-space point design (TSPD). The scale-up progressed from small-scale lap shear coupons to a 3-ft-long subelement structure representing the most highly loaded joint in the TSPD. Through the scale-up effort, numerous welding trials were conducted to develop a suitable approach. While the intended application is an in-space welding operation, the scale-up effort was conducted in a lab environment due to project resource constraints.

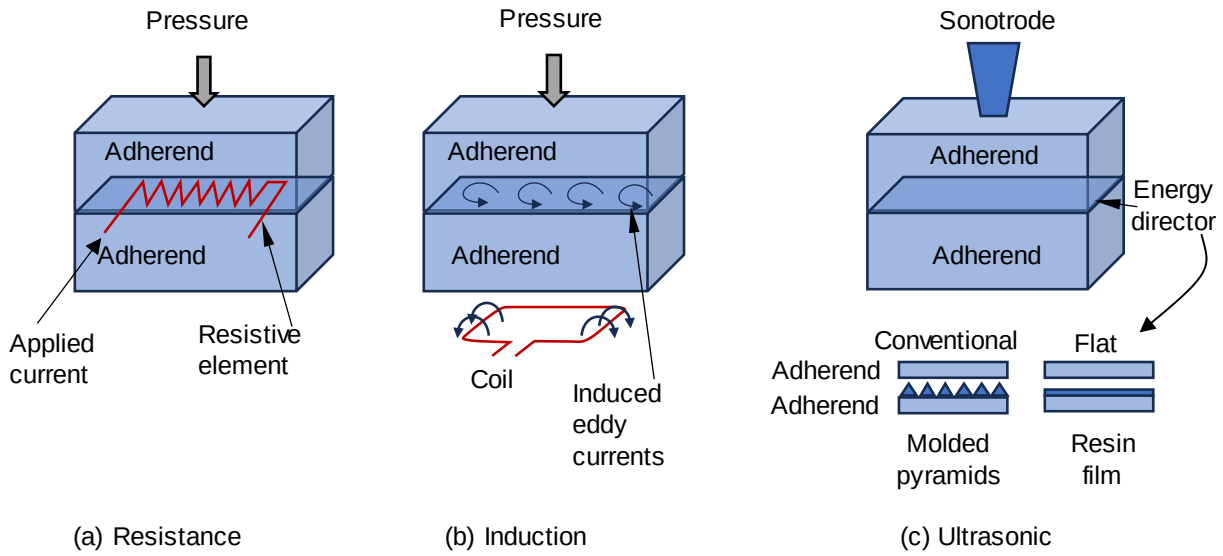


Figure 1. Schematics of welding methods considered in this study.

Relatively little work has been done to advance TPC welding capability for in-space applications. To the authors' knowledge, there is no published data on TPC welding in a simulated space environment including in vacuum, cold temperature, or microgravity. Most of the weld evaluations TDEA completed were conducted in a lab environment. TDEA planned welding trials in cold temperature and vacuum, but this work was descoped due to early termination of the project. Nonetheless, TDEA still conducted numerous welding trials working toward developing the technology for eventual in-space applications. This report provides an assessment of the potential for TPC welding in-space based on the experience and data collected by the TDEA project, as follows:

- Section 2: Summary of TDEA's coupon-scale welding trials including resistance, induction, and ultrasonic welding methods. Weld process and performance data are reported in section 2.1 to establish the basis of a welding method assessment that follows in section 3. The following exploratory studies are also described:
  - 2.2: Resistance welding studies assessing a double lap shear configuration, dissimilar material welding, heating element variations, and reproducibility;
  - 2.3: Resistance and ultrasonic welding studies assessing thin-ply adherends;
  - 2.4: Ultrasonic welding studies assessing additive and automated fiber placed adherends;
  - 2.5: Ultrasonic welding scale-up trials targeted toward a large-scale TDEA truss tower application including thick adherends, directional adherends, and enlarged bond areas.
- Section 3: An assessment of the advantages, limitations, and development needs for the three weld methods.
- Section 4: Considerations for TPC welding in-space, including:
  - 4.1: Material properties related to outgassing, CTE, and cold temperature effects;
  - 4.2: Ultrasonic welding trials with regolith simulant contamination;
  - 4.3: Reassembly trials.
- Section 5: Structural subelement demonstration of an ultrasonic welded joint including:
  - 5.1 Test article design;
  - 5.2 Finite element modeling;
  - 5.3 Truss element manufacturing;
  - 5.4 Subelement welding processes and parameters;
  - 5.5 Nondestructive evaluations;
  - 5.6 Test setup and procedures;
  - 5.7 Test and analysis results.

The overall experience in TDEA suggests well-controlled and repeatable heat and pressure application are imperative to produce high-quality welds. The data summarized herein suggest TPC welding is a viable candidate for in-space structural assembly, but further work is needed to demonstrate this technology in actual space environments and to build confidence in process repeatability.

# 2 Small-Scale Welding Trials

This section describes several welding trials conducted in the TDEA project that provide a basis for the evaluation of the advantages, limitations, and development needs. All welding trials were completed in a lab environment.

## 2.1 Weldability study

The first welding trials, denoted as the "weldability study," included the resistance, induction, and ultrasonic weld methods applied to produce single lap-shear (SLS) specimens and double cantilever beam (DCB) specimens. The SLS and DCB test specimens loosely followed ASTM D5868 [11] and ASTM D5528 [12], respectively. The weldability study was proposed as an effort to generate data for evaluation of how different weld methods and materials interact, based on the assumption that relatively well-consolidated joints could be readily produced with minimal process development. The SLS specimens used 16-ply quasi-isotropic (QI) substrates and specified a 1.0 in. x 1.0 in. overlap. The layup used was $[45/0/–45/90]_{2s}$ such that the weld interface was between 45° plies. Each specimen was welded individually with the target weld extending over the full 1.0 $in^2$ overlap area, as shown in Figure 2. The rationale for welding individual specimens was to focus on spot welds relevant for assembling truss structures with lap joints (see Section 5). Likewise, DCB specimens were welded individually, but used a unidirectional layup for resistance and ultrasonic welding. Induction welding of DCB coupons was attempted with substrate laminates having some off-axis plies within the arms but was ultimately unsuccessful due heating challenges. The resistance welded DCBs were produced using sequential 1.0 in. x 1.0 in. welds. In general, the DCB tests for mode I fracture toughness were mostly unsuccessful or yielded data challenging to interpret due to weld-induced defects that lead to non-self-similar or unstable fracture propagation. As a result, the DCB test results are not described further in this report. Future work is needed to address challenges associated with fracture toughness characterization.

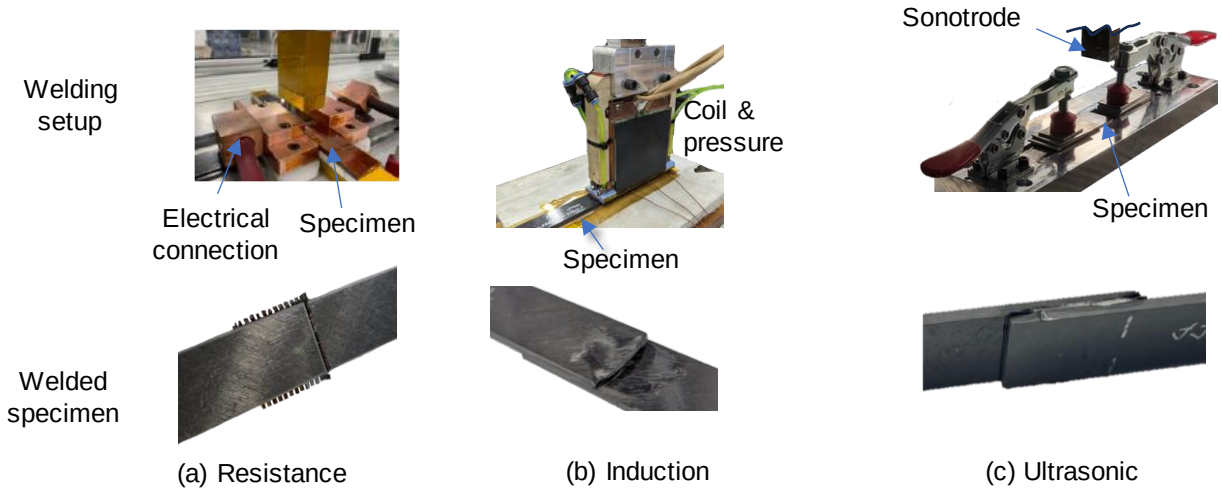


Figure 2. Summary of weldability study welding setups and photographs of welded specimens.

Each welding method was performed by a contracted welding organization: National Institute for Aviation Research (NIAR) for resistance, Spirit AeroSystems Holdings, Inc. for induction, and Agile Ultrasonics Corp. for ultrasonic. Each weld setup and process are unique and tailored by the welding organization. The weld setups are

described in the weldability study report [13], but a brief description is provided here. Resistance welds were conducted using a dry T300 plain-weave-fabric carbon fiber heating element with 3K tows. The heating element was sandwiched between layers of resin film (same polymer as adherend matrix) and then the adherends. Current was applied to the heating element through copper terminals and static pressure was applied using a pneumatic cylinder. Shims and the terminals provided support around the perimeter of the weld to maintain pressure while the material melted. The welding recipe was developed through trial welds with an embedded thermocouple where the power was controlled to yield a prescribed temperature history (temperature feedback, closed loop control scheme). Subsequent welds used the same power history without thermocouples. Additional details on the resistance welding are available in [14, 15]. Induction welds were performed using a stationary, water-cooled coil and no additional material placed at the weld interface. The coil was encased in a fixture that was used to simultaneously apply pressure. The specimen was placed in a purpose-built tool that fixed the adherends in place. Ultrasonic welds used a support tool with similar geometry as the induction welds and the setup included clamps. The ultrasonic welds were completed without an additional material (i.e., no energy director). The welding was done with high-amplitude 20 kHz ultrasonic vibrations applied for a relatively short duration as the sonotrode scanned across the overlap region. For the commercially available standard-ply-thickness material systems, adherends were consolidated in a heated press and preparation was limited to a solvent wipe for all weld methods. Typical adherend surface roughness was around 32 RMS.

The weldability study was conducted with five unidirectional prepreg material systems, as summarized in Table 1. Four of the material systems are commercially available standard ply thickness high-performance carbon fiber reinforced thermoplastics. These four material systems were the primary focus of the weldability study, and more details are available in [13]. A fifth thin-ply material system was also considered. These material systems were selected to represent a variety of candidate resin systems, and based on availability at the start of the project. The considered resin systems were LM-PAEK (low-melt polyaryletherketone), PEEK (polyetheretherketone), PPS (polyphenylene sulfide), PEI (polyetherimide), and PEKK (polyetherketoneketone). PEI is amorphous while other resins are semi-crystalline. The considered carbon fibers were T700GC, AS4, and M30S. While the fibers are not typical for most space structure applications (TPC prepregs with high-modulus carbon fiber were not commercially available), the resin systems are considered representative. The PEKK/M30S is a thin-ply material form that was produced by NASA's Deployable Composite Boom project [16]. Results for the PEKK/M30S specimens are presented in this section, and a dedicated discussion of the results is provided in Section 2.3. Prior to completing the deliverable welds used for evaluation, the welding organizations were provided additional substrates to use for process development. The number of substrates available for each welding method and material system varied but was essentially the minimum number requested by the welding organization. After process development, approximately 10 welds were completed with the same welding recipe for each material and welding method. The welds were evaluated by nondestructive evaluation (NDE) including ultrasound and X-ray computed tomography (XRCT), mechanical test, and differential scanning calorimetry (DSC). Lap-shear strengths (LSS) are reported from the mechanical tests assuming a bond area of 1 $in^2$ except where noted otherwise.

Table 1. Material systems used in the weldability study.

| Resin | Fiber | Material Designation | Vendor | Fiber Areal Weight oz/ft$^2$ (g/m$^2$) | Resin Weight Percent (%) | Ply Thickness in. (mm) |
|---|---|---|---|---|---|---|
| LM-PAEK | T700GC | TC1225 | Toray | 0.475(145) | 34 | 0.0054 (0.137) |
| PEEK | AS4 | TC1200 | Toray | 0.475 (145) | 34 | 0.0056 (0.142) |
| PPS | AS4 | TC1100 | Toray | 0.724 (221) | 34 | 0.0083 (0.210) |
| PEI | AS4 | APC/TC1000 | Toray/Solvay* | 0.475 (145) | 32 | 0.0052 (0.132) |
| PEKK | M30S | M30S/PEKK | Osaka | 0.121 (37) | 37 | 0.0014 (0.036) |

* Solvay material was used for most of the specimens. Toray material was used for the results presented in Sections 2.2.1 and 2.2.2.

The key findings from the weldability study include observations and characterization of common welding defects in heat affected zone (HAZ), quantification of apparent LSS and the associated coefficient of variation (COV), and improved understanding of the role of edge effects in the welding methods and their impact on the results. A wide range of LSS were found, as shown in Figure 3. Overall, resistance welds were the strongest and ultrasonic welds were the weakest.

Defects, such as unwelded regions, delamination, porosity, or distortion (thinning, fiber pushout) occurred in the HAZ for all weld methods and material combinations, but the extent of defects varied. Defects were measured by NDE and verified by microscopy and posttest evaluations. In general, where the welding organization had substantial previous experience with the material system (e.g., NIAR resistance welding AS4/PEEK TC1200) the extent of the defects, was lower and the LSS was higher. When tasked with welding a material for which the welding organization had less heritage, the defects were much more extensive (e.g., AS4/PPS for all weld methods) and the LSS was lower. This suggests that the process development efforts allowed for in this study were generally insufficient. Numerous process development trials are required to obtain few defects no matter the weld method and material system. However, as discussed throughout this report, strong welds were not necessarily defect-free.

High COVs were found in the LSS data, mostly >10%, as shown in Figure 3. The COVs were consistent with the defect observations in that 1) configurations with defects located near the reentrant corners (high stress region) tended to have lower LSS compared with configurations where defects were located in the middle of the overlap (low stress region), and 2) higher variation in observed defects correlated with higher LSS COV. In general, the resistance weld defects were located near the center of the overlap, whereas the induction and ultrasonic weld defects occurred near the ends of the overlap, which may explain why the LSS were the highest for resistance welding. The strength data may also be affected by the effects of incomplete healing or crystallization across the weld interface, which is not captured in the NDE or microscopy data. Even among cases where the COV is less than 10%, evidence of defects with variability among the nominally identical replicates was observed, e.g. resistance welding with PEI [14].

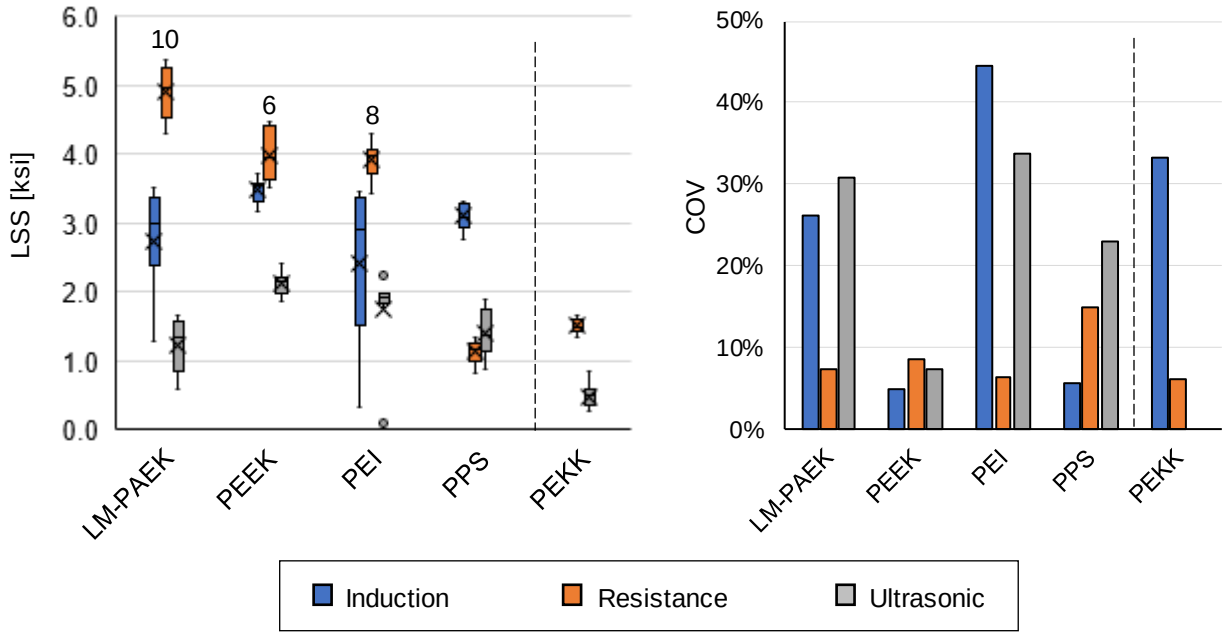


Figure 3. Summary of LSS and associated COV from the weldability study. On the left, the number of replicates for each case was 9 except as indicated differently by a number above the dataset. The mean values are indicated with × symbols and outliers are shown with circular markers. The dashed line segregates the results for the thin-ply material, which had a thinner laminate.

Photomicrographs, NDE, and evaluation of the failure surfaces reveal some insights into the welding processes. Photomicrographs are summarized in Figure 4 and NDE and failure surface images are available in [13]. Overall, fiber pushout near the corners was nearly universal. Induction and ultrasonic welding were more likely to introduce porosity and delaminations but porosity was observed in some resistance welds. The PEI adherends apparently had some porosity prior to welding, which may have influenced the welding results. The PPS surface plies had relatively uniformly spaced matrix cracks, perhaps due the thermal residual stresses and relatively large ply thickness. Fiber tear type failure modes were typically observed for welds with higher LSS. Welding to the edge of relatively small specimens was identified as a challenging configuration, particularly for induction welding and ultrasonic scan welding. For induction welding, the eddy currents try to form a closed loop and so the tool-part interaction is important to get controlled heating to the edge of the part. In ultrasonic welding, when the sonotrode (horn) is scanned over such a small area, transient start-up and stop process parameters are critical. Likewise, excess heating can occur near the edge from wave propagation or tool-part interaction. Ultrasonic welding in a plunge configuration where the sonotrode remains fixed may be more appropriate for the weld application considered in the weldability study and is discussed later in this report.

In summary, the weldability study revealed the three welding methods, in the configurations considered, require additional process development work to produce well-consolidated and repeatable welded joints. While some thermoplastic composite welding has reached Technology Readiness Level (TRL) 9 for some specific aircraft applications and material systems (e.g., [17]), broad knowledge of these welding processes applied to the configurations considered herein is still missing.

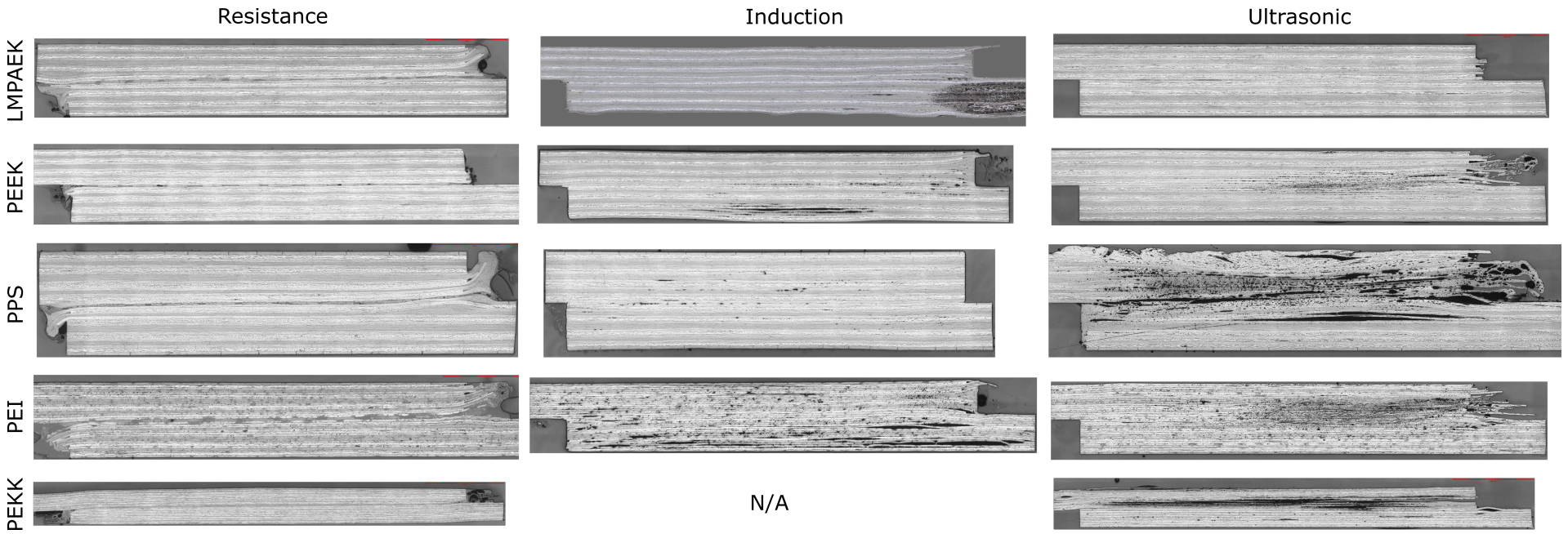


Figure 4. Representative photomicrographs of SLS welds taken at mid-width of the specimen, showing observed weld defects including: porosity, fiber pushout, thinning, and delaminations.

During process development for the ultrasonic welds, SLS welds were conducted with different combinations of three process parameters: scanning speed, clamping force, and sonic amplitude. LSS from these welds provided data to study the relationships between these process parameters and mechanical performance. A data-driven modeling approach, Gaussian process regression (GPR) was employed and is described in Appendix A. The results show that relatively sparse and noisy data is difficult to interpret. With additional test data, this modeling approach has the potential to help quantify process uncertainty and inform decisions about where to focus within the large process parameter space.

## 2.2 Additional resistance welding trials

Some additional coupon-scale resistance welding trials beyond the scope of the weldability study were completed, including 1) double lap welds, 2) welding PEEK to PEI, 3) welding with different heating element configurations, and 4) in-house welding with AS4/PEEK. The results of these efforts are briefly described in the following sections.

### *2.2.1 Double lap shear*

Double lap-shear resistance welds were evaluated to assess the manufacturing differences compared with SLS welds. Specimens were manufactured and tested for PEEK and PEI material systems, loosely following ASTM D3528 [18]. The two welds were made sequentially. The process development showed that two separate processes were needed for the first and second welds. In general, the strengths were relatively low and much more extensive porosity was exhibited in the double lap-shear welds compared with SLS welds, Figure 5. Hence, future work is needed to mature double lap welding procedures.

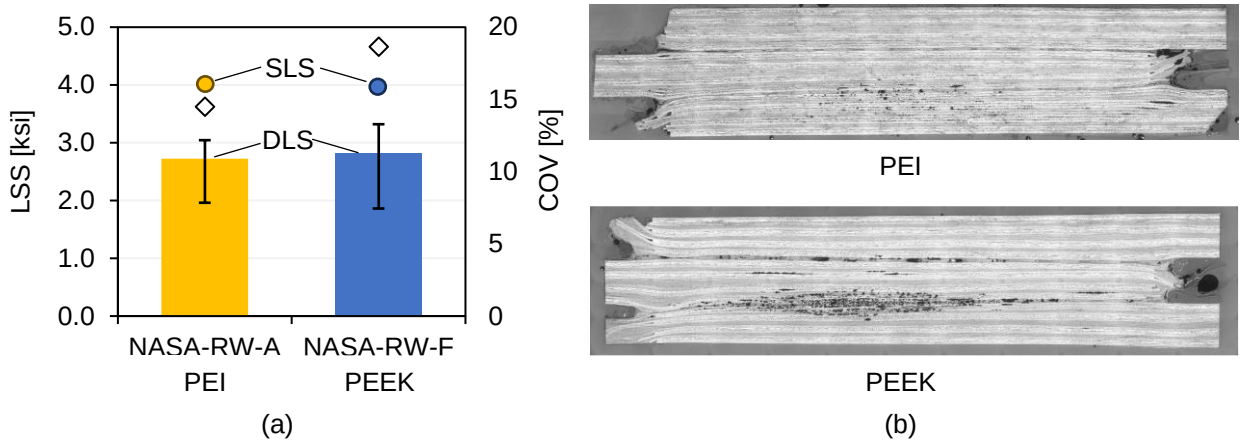


Figure 5. (a) LSS and (b) representative photomicrographs from double lap-shear (DLS) welds. Error bars in (a) show min and max values for n=6 and the COV is indicated by the diamond markers. The circle markers show the mean SLS LSS repeated from the weldability study. Note that extensive fiber pushout in (b) can be mitigated to some extent by improved tooling concepts. The porosity in (b) is suspected to be due to local overheating.

### *2.2.2 PEEK to PEI hybrid*

Resistance welds between PEEK and PEI 16-ply QI laminates were completed on three SLS specimens at NIAR to assess the feasibility of hybrid joints. In these welds, a $[0/–45/90/45]_{2s}$ layup with 0° plies at the weld interface was used. Two different resin films were used on either side of the heating element, matching the material of the adjacent adherend (i.e. PEI film on the side with the PEI adherend and PEEK film on the side with the PEEK adherend). The welding was done with the weld recipe targeting 725 °F at the weld interface. The processing temperatures used for the PEI and PEEK single-material welds were 625 °F and 725 °F, respectively, and the manufacturer recommend maximum temperature for processing the PEI is 660 °F. So, the PEI was slightly overheated to ensure the PEEK was heated sufficiently. The average LSS was 2.4 ksi with a very low COV of 1.0%. This LSS is about 80% and 55% of the non-hybrid PEI and PEEK LSS, respectively, showing there is some appreciable knockdown for a hybrid joint. This result confirms the possibility of resistance welding to join PEEK and PEI based laminates as previously reported in the literature (e.g., [19]).

### *2.2.3 Carbon fiber heating element permutations*

Alternative carbon fiber heating elements were evaluated to determine the sensitivity of the welding process and joint mechanical performance to the heating element. The baseline heating element used in the weldability study is a plain weave T300 carbon fiber fabric with 3K tows with the tows parallel to the loading direction removed in the joint overlap region, as shown in Figure 6a. Three alternative configurations were evaluated: 3K fabric with no tows removed, and 1K fabric with and without tows removed, as represented in Figure 6b–d. Five SLS replicates were welded at NIAR for each heating element configuration using 16 ply QI adherends made from TC1225 (T700/LM-PAEK). Resin films were used for all variants.

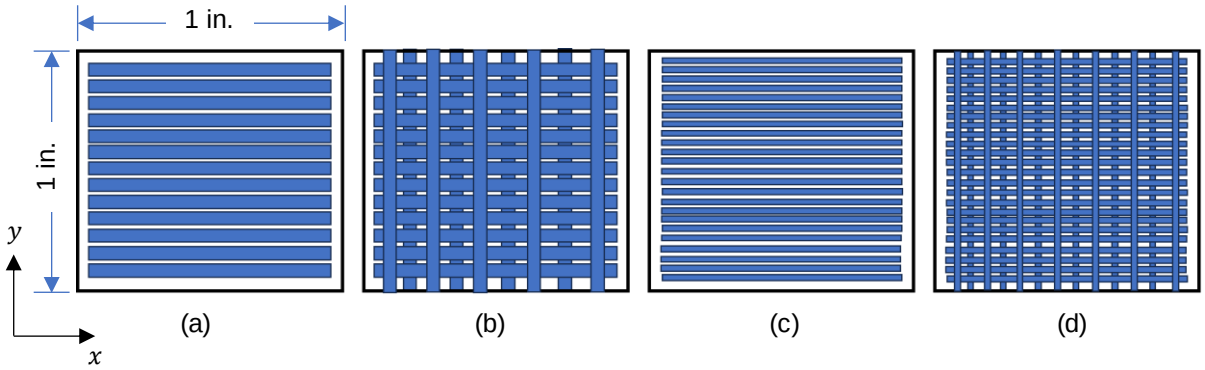


Figure 6. Schematics of heating element tow layouts in the joint overlap region (note that the plain weave interlacing of the tows is not shown in this schematic). The heating element is made from a plain weave carbon fiber fabric and extends beyond the 1 in. shown in the $x$-direction for clamping to the electrodes. The specimens are loaded in the $y$-direction. In (a) and (c), the $y$-direction tows are removed.

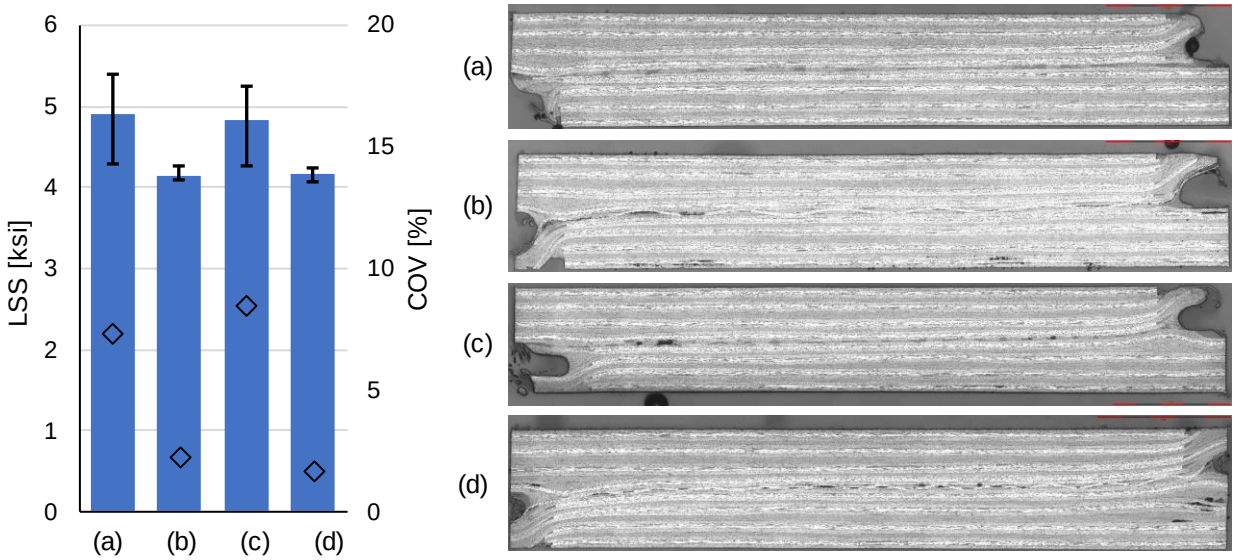


Figure 7. LSS and representative photomicrographs of SLS specimens resistance welded with different heating element configurations shown in Figure 6. The LSS error bars show min and max values with n=3 for (b)–(c) and the COV is indicated by the diamond markers.

The LSS results, Figure 7, show removing the tows parallel to the loading direction, cases (a) and (c), led to higher strength joints. It was also observed that these heating elements produced smoother temperature and resistance

histories. However, it is interesting to observe that the scatter tends to be higher. Little difference in LSS is noticed comparing the heating elements with 3K and 1K tows. The photomicrographs show evidence of more voids near the heating element when 1K tows are used, (c) and (d). Overall, all permutations of resistance welding with different heating elements performed well. Alternative tests, such as fracture toughness characterization tests, could be considered in future work to further probe the effect of various heating elements on the joint performance.

### *2.2.4 In-house welding trials*

A resistance welding setup emulating the setup at NIAR was built at Marshall Space Flight Center (MSFC) to get hands-on experience with thermoplastic composite welding within NASA. The MSFC setup was modeled on the NIAR setup and thus very similar. Dozens of trials were conducted using AS4/PEEK 16-ply QI substrates with the aim of obtaining a repeatable process. Despite the extensive effort, significant variability in thermal history was found in nominally identical welding trials. These data are unique in the TDEA project in that they offer the only insight into the repeatability of the temperature history during welding. The significant variability observed in the temperature history data appears to correlate with the variability in joint outcomes in terms of defects and strength.

## 2.3 Results for resistance and ultrasonic welding of thin-ply laminates

Thin-ply materials are beneficial for some space structure applications. While at the time of this effort, commercial thin-ply thermoplastic composite prepregs were not available, some thin-ply material was provided from the NASA Deployable Composite Boom project for welding evaluation, Table 1.

The adherends were cut from panels with a $[45/–45_2/45/0/90_2/0]_{2s}$ layup. Note that, despite having 32 plies, the final adherend thickness was 0.05 in., which is roughly half the typical adherend thickness for other materials evaluated in the weldability study. Manufacturing the panels using the thin-ply material was challenging because of the difficulty tacking the tape in place, and its brittle nature in that it easily split longitudinally. Consequently, groups of four symmetric and balanced plies were laid up and then iteratively run through a press cycle to obtain initial consolidation. Once the layup process was complete, the panel was consolidated using an autoclave with 500 psi applied pressure. Cycles with lower pressure (< 250 psi) were tried but lead to high porosity within the laminate plates.

The resistance and ultrasonic welding procedures mostly followed the approaches described in Section 2.1. During initial resistance welding process development, adhesive-type failure (decohesion at the welded interface) was observed. To prevent adhesive failure, the faying surfaces were hand sanded and the applied pressure during welding was increased to 560 psi from 100 psi. With this updated procedure, failure surfaces showed evidence of cohesive failure mode (failure within the layers) and fiber tear, indicating a higher strength weld. This improved process was used for all tested and inspected weld data reported herein. Resin films were used on either side of the heating element.

The LSS data were shown previously in Figure 3, where it is evident that relatively low values were achieved. Thinner laminates introduce higher peel stresses due to bending, which may explain the relatively low LSS to some extent. Photomicrographs are shown in the bottom row of Figure 4 and illustrate relatively few defects in the resistance weld and numerous defects in the ultrasonic weld. Additional work is needed to develop an ultrasonic welding process suitable for such thin-ply laminates.

## 2.4 Ultrasonic welding of laminates produced by automated fiber placement (AFP) and additive manufacturing (AM)

A manufacturing concept of interest for TDEA involved TPC welding of additive manufacturing (AM) components to conventionally manufactured components, for example parts manufactured by automated fiber placement (AFP). AM can be an efficient manufacturing strategy for parts with complex geometries, particularly for low-quantity parts that have significant tooling cost. AM also has relevance for robotic assembly for both in a terrestrial environment and in space.

Ultrasonic welding, NDE, photomicroscopy, and mechanical testing were performed at NIAR on a set of AM-to-AFP SLS specimens along with a set of AFP-to-AFP SLS specimens as a baseline for comparison. Six SLS welds were prepared for each configuration and inspected via ultrasonic NDE, with one SLS specimen from both sets destructively cross-sectioned and the remaining five SLS specimens from both sets mechanically tested. The AM

adherends were 3D printed from QI AS4/LM-PAEK and post-machined to reduce surface roughness by Mantis Composites, Inc. The final dimensions were 4.0 in. x 1.0 in. x 0.1 in. The AFP adherends were also 4.0 in. x 1.0 in. x 0.1 in. and made from 16 plies of QI T700/LM-PAEK. Ultrasonic welding was conducted over a 1 in. x 1 in. overlap area with a stationary 1.0 in. x 1.0 in. sonotrode. For the AM-to-AFP welds, the AM adherend was positioned on top in contact with the sonotrode. A 0.008-in.-thick mesh film of LM-PAEK was used at the weld interface as an energy director (ED). An ED is typically a resin layer with a rough surface which helps localize heating at the interface

The AM-to-AFP and AFP-to-AFP LSS and corresponding COV are shown in Figure 8. The baseline AFP-to-AFP welds had more than double the average LSS of the AM-to-AFP welds, as well as significantly lower variability (COV 3.5% for AFP-to-AFP, 17.6% for AM-to-AFP). The reduced strength of the AM-to-AFP welds is correlated with increased deconsolidation that was observed from both ultrasonic NDE and cross-sectional photomicroscopy as shown in Figure 9. The AM adherends had high porosity prior to welding (approximately 3.0 ~ 3.5 vol% measured via micro XRCT). These voids may dissipate ultrasonic wave energy as heat, and if the material is overheated, deconsolidation occurs. This may explain the deconsolidation observed away from the weld line in the photomicrograph. Possible strategies for mitigating this deconsolidation could include reversing the order of the adherends so the low-porosity AFP material faces the sonotrode, a separate post-print consolidation step for the AM adherend prior to welding, or selecting a different weld approach such as resistance welding.

It is interesting to compare the AFP-to-AFP ultrasonic weld results with the results obtained in the weldability study. Here a LSS of 5.48 ksi is obtained whereas in the weldability study with LM-PAEK, the LSS is 1.2 ksi. The difference is likely attributable to the differences in welding setup, which were numerous because the welds were completed by two different organizations each with their own custom welding configurations. However, it is noteworthy that in [20], 1.9 ksi and 5.3 ksi are reported for LSS with no energy director and with a mesh energy director, respectively. This result, consistent with the results presented here, suggests that the energy director is the key factor explaining the difference in LSS. For the AFP-to-AFP welds, the NDE results show evidence of defects (Figure 9), which is surprising considering the relatively high LSS with low COV. The AM-to-AFP weld NDE shows extensive defects, consistent with high porosity in the AM adherends and the microscopy data.

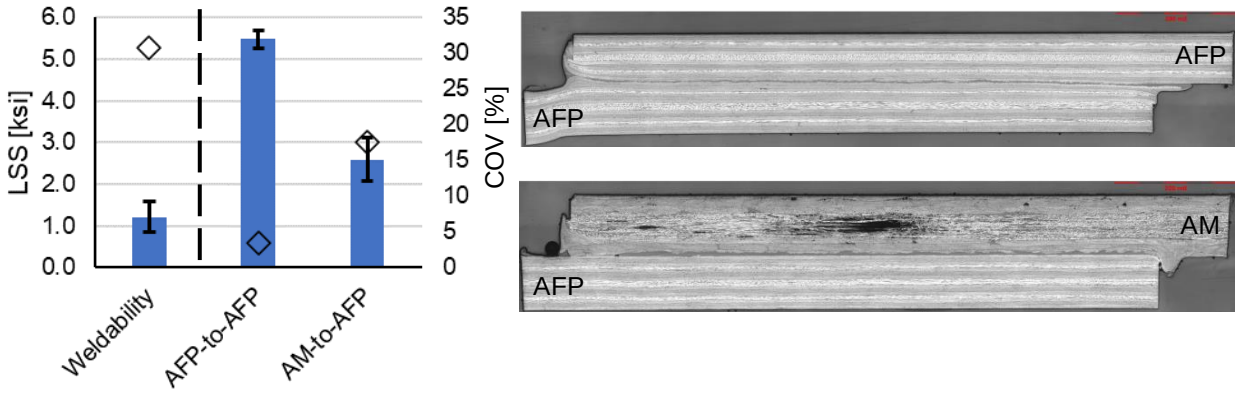


Figure 8. (a) LSS and (b) representative photomicrographs (specimen replicate C, along mid-width). (a) Mean LSS is reported (n=5) with error bars showing ±1 standard deviation and the COV is indicated by the diamond markers. The results labeled “Weldability” are repeated from section 2.1.

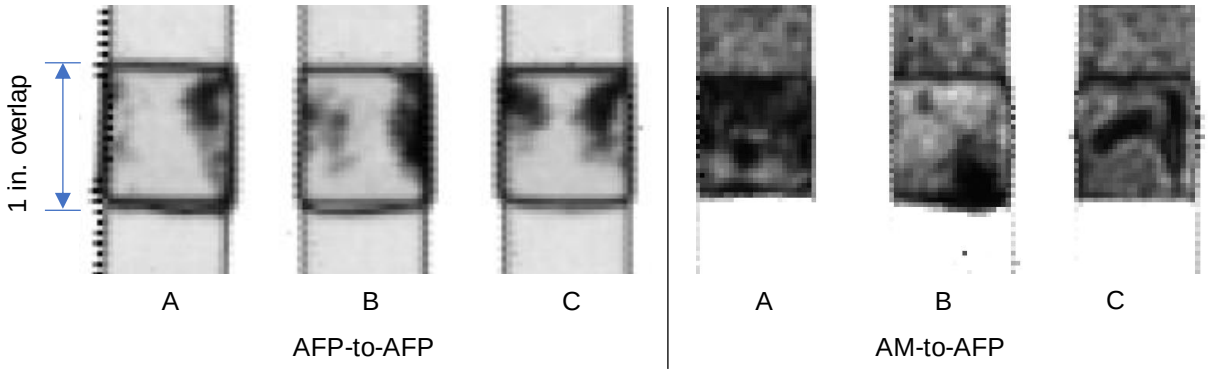


Figure 9. Through-transmission ultrasonic C-scans for the three replicates (A–C) each of LM-PAEK AFP-to-AFP and AM-to-AFP welds. Light-gray regions are high amplitude and consistent with good consolidation, while dark regions indicate potential defects. The defects are mostly concentrated along the left and right edges of the weld overlap region in the AFP-to-AFP welds and throughout the AM-to-AFP welds and AM adherends.

## 2.5 Ultrasonic weld iterations toward scale-up

The scale-up efforts focused on the TSPD subelement test article (see section 5) to demonstrate the feasibility of using the welding technology. The TSPD subelement fabrication involved significantly thicker adherends with 0° dominated layups, and a significantly larger bonding area. Ultrasonic welding of T700/LM-PAEK was down-selected for the TSPD application prior to having the weldability study data due to project schedule constraints. To facilitate this welding scale-up, several iterations of weld recipe optimization were undertaken at Agile Ultrasonics with the goal of achieving fully consolidated and strong welds. These welds were with one-inch-wide specimens except where noted otherwise. Although autoclave consolidated baseline data was not available, for T700/LM-PAEK 16-ply QI adherends, a strong weld is assumed to have an LSS ≥ 5 ksi (see Figure 7 and Figure 8).

LSS results for trials (1–5) conducted using 16-ply QI substrates are summarized in Figure 10a. Trial 1 shows the results from weldability study process development corresponding to the best recipe, which was subsequently applied in the weldability study. Trial 2 is the result from the weldability study (same as shown in Figure 3). Trial 3 was conducted using substrates laid up by AFP and the welding fixture was updated to improve pressure application during welding. Trial 4 is nominally identical to trial 3, and highlights that the variability in the data persists. Trial 5 includes an approximately 0.0024-in.-thick LM-PAEK film at the weld interface (i.e., a flat ED). The ED was expected to yield an improvement in LSS based on data reported in the literature. However, no significant LSS improvement was obtained with the ED. NIAR achieved more than twice the LSS for AFP laminates (Figure 8), however, the welding setup and process parameters were much different than those used for the welds reported in Figure 10.

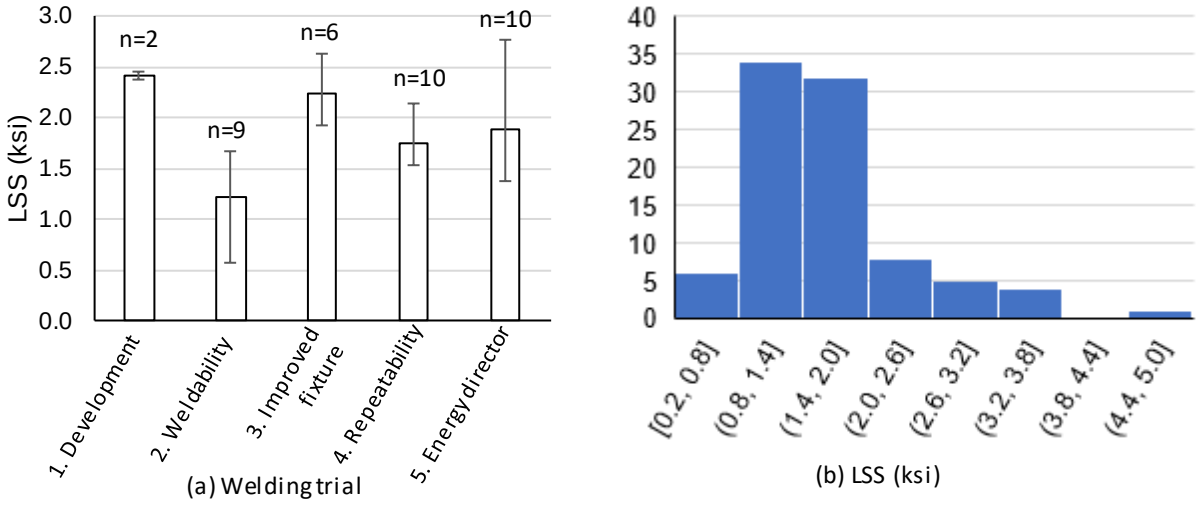


Figure 10. (a) LSS from five trials of ultrasonic welding processes arranged chronologically from left to right and (b) histogram of thick-adherend LSS illustrating most recipes yield less than 3 ksi LSS.

The remaining ultrasonic weld iterations were conducted using thick substrates with a 0°-dominated layup representative of the TSPD application. This scale-up testing progressed driven by project schedule constraints despite limited understanding of the factors affecting LSS and its relatively high COV. For these subsequent welds with thick adherends, a wide variety of welding recipes were considered with relatively few replicates used for each condition to cast a wide net toward identifying a promising approach. The following weld parameter variations were tested:

1. One or four layers of a 0.0024-in.-thick LM-PAEK film (i.e., flat) ED;
2. With and without preheating the lower adherend to 350 °F;
3. Static force ranging from 104 to 146 lbf;
4. Variations in sonic amplitude and weld time;
5. Post-weld dwell time of 0 to 60 seconds;
6. Scanning or plunge configurations;
7. Fixture variations for clamping and positioning.

TDEA project nomenclature for these welds is based on a naming convention that was established by Agile Ultrasonics and the weld test data are referred to as task 5.4, task 5.6, and task 6.2. The welds in task 5.4 were scan welds with a 1.0 in. x 1.0 in. overlap with both adherends being 52-plies thick, with a layup of $[45/90/–45/0_{13}/45/90_2/–45/0_6]_s$. The welds in task 5.6 and 6.2 were stationary plunge welds with a 1.0 in. x 1.5 in. overlap such that the 0.5 in. x 1.0 in. sonotrode had a 0.25 in. offset (setback) from the edge of the specimen around its perimeter. This offset of the weld from the specimen edges (setback) was thought to be more representative of the planned approach for scale-up weld application. The welds presented in task 6.2 had different adherend thicknesses and layups. One adherend was 52-plies thick (same as previous cases) and the other was 60-plies thick, $[(45/0_3/–45/0_2)_4/0_2]_s$. The LSS are shown together in a histogram in Figure 10b to emphasize that most of the strength data are less than 3 ksi. As the adherend flexural rigidity increases, the LSS for equivalent interface properties increases. For instance, the LSS for 52-ply 0-degree-dominated laminate adherends is predicted to be about 60% higher than the LSS with 16-ply QI adherends assuming equivalent interface properties [21]. Based on the described weld trials, the TDEA project selected plunge welds with four layers of resin film as an ED, high force and post-weld dwell to encourage consolidation, and amplitude and weld-time bias toward overheating vs. underheating the joint because overheating could still lead to a strong joint while underheating risked a very weak connection. Note this rationale was qualitative in nature; no quantitative and repeatable relationships between weld parameters and LSS were established.

While the relationships between welding parameters and weld outcomes remained elusive, overall, it appears stronger ultrasonic welds were achieved when more energy was input. Although erroring toward too much energy input likely led to overheating and polymer degradation (as evidenced by smoking during welding and adherend delamination), the LSS data suggests strong joints can still be formed. In contrast, underheating is undesirable in that it can lead to very weak joints. XRCT scans were completed on selected welds, and an evaluation of weld quality was attempted, for task 5.6 welds. Figure 11 shows a comparison of specimen TDEA-441-02-SLS-AB that appeared to be a "good" weld via NDE in that it was well consolidated with relatively few voids in the middle. This is contrasted against TDEA-441-02-SLS-AQ, which is one of the strongest welds scanned by XRCT and more representative of the typical inspection result among the task 5.6 welds. Specimen TDEA-441-02-SLS-AQ exhibited delaminations in one of the adherends and a significant region that is not welded, evident by the gap between the adherends. The LSS values are reported in Figure 11 for the two specimens, and show the apparently well consolidated weld -AB was one of the weakest tested (comparing back to Figure 10b). This result may be attributed to the lack of polymer chain entanglement across the weld interface being undetectable by conventional inspection (i.e., the classic weak/kissing bond problem, common in adhesive bonding). Further research is needed to understand the weld consolidation process and the relationship between LSS and welding parameters.

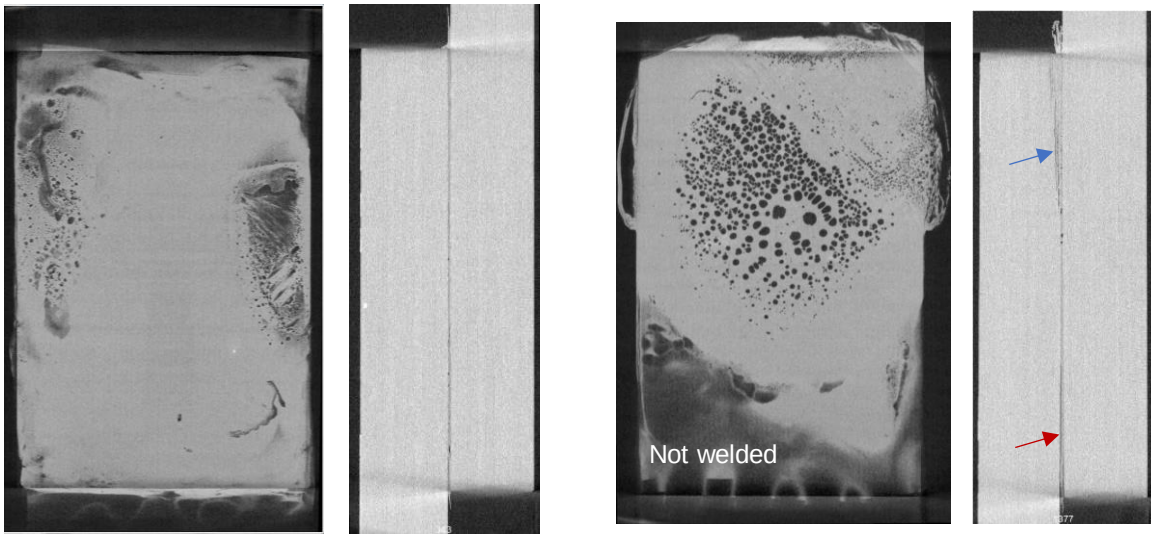


Figure 11. Two examples of XRCT results showing plan views of the weld interface (minimum projection between adherends) and side views at a location through the width. The blue arrow points to adherend delamination and the red arrow points to a gap between the adherends, which is showing the same information as the viewed in the plan view (labeled 'not welded').

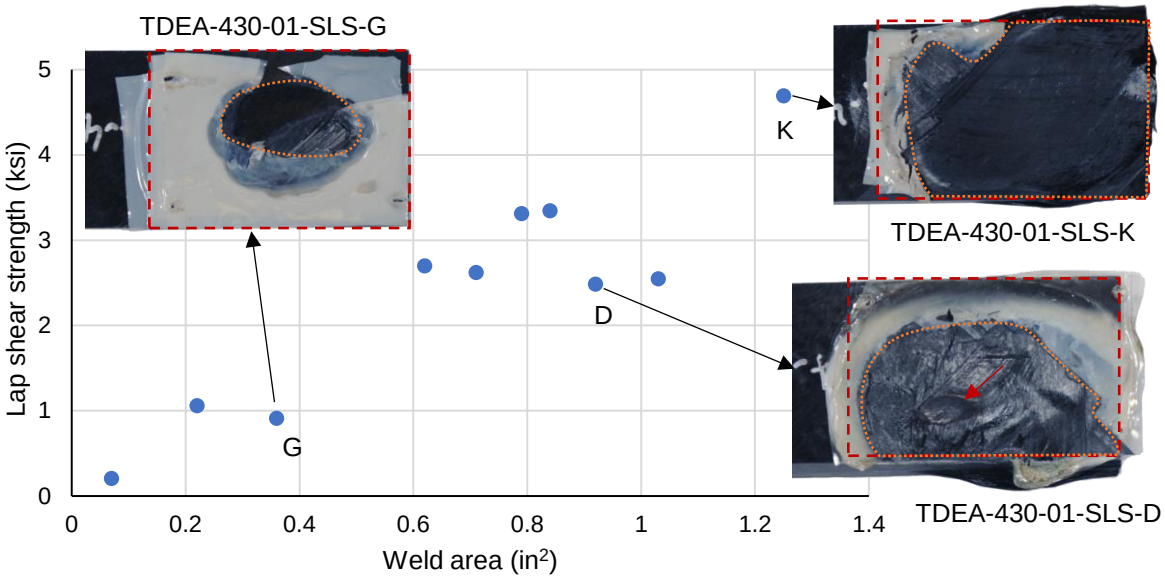


Figure 12. LSS correlation with welded area measured from posttest failure surface images and three examples of failure surface images. The red dashed box shows the 1 in. x 1.5 in. overlap area. The orange dotted lines identify the regions where the material was successfully welded (welded area).

Failure surface images show evidence of the welded region and some indications of the temperatures reached during the weld process. For example, in regions where the polymer film layers are unbonded, the maximum temperature likely did not exceed the polymer's melting temperature. Overall, the welded area shows a relatively linear relationship with LSS, as shown in Figure 12. Weak LSS is likely due to smaller welded area, which results from incomplete welding, instead of adherend degradation/delamination in the HAZ[1]. Examples of failure surface photographs are shown in Figure 12 for three specimens with a range of welded area. In unwelded regions, the resin film remains intact. In welded regions, the failure mode is fiber tear. In the case of specimen -D, there is brown discoloration (red arrow), which suggests resin degradation (overheating) occurred.

Finally, the ultrasonic welding approach was trialed on larger SLS specimens to gain experience with creating a larger weld area using multiple passes or a sequence of stationary plunge welds. These specimens were referred to as the weld setback coupons since they included an intentional standoff distance from the target weld area to the specimen edge, which was intended to mitigate fiber pushout and as representative of the configuration planned for the following TSPD sub-element welds. The specimen configuration is shown in Figure 13. For the weld setback coupons, the weld recipe (collection of weld parameters) was still being developed when these specimens were welded and so different weld parameters were used. Five welds were made with three adjacent scans and six welds were made with a series of plunge welds. The scan welded specimens were welded with one layer of 0.0024-in.-thick LM-PAEK film and no preheating. The plunge welded specimens were welded with four layers of 0.0024-in.-thick LM-PAEK film and the adherends were preheated to 350 °F prior to welding. The specimens showed similar characteristics to the smaller scale SLS specimens. The maximum loads are shown in Figure 14 as a function of weld area determined

[1] In other loading configurations (e.g., out-of-plane), adherend delaminations in the HAZ may be more critical.

from posttest failure surfaces. Overall, the target 4.5 $in^2$ weld area was not achieved in any specimen, and consequently the joint strengths were relatively low. The lack of complete welding was attributed to inadequate clamping and fixturing. The primary outcome of these weld setback specimens was to identify a welding recipe based on the LSS that would be used for the TSPD sub-element welds. However, it turned out that different welding parameters were required for the TSPD sub-element welds, likely due to differences in fixturing.

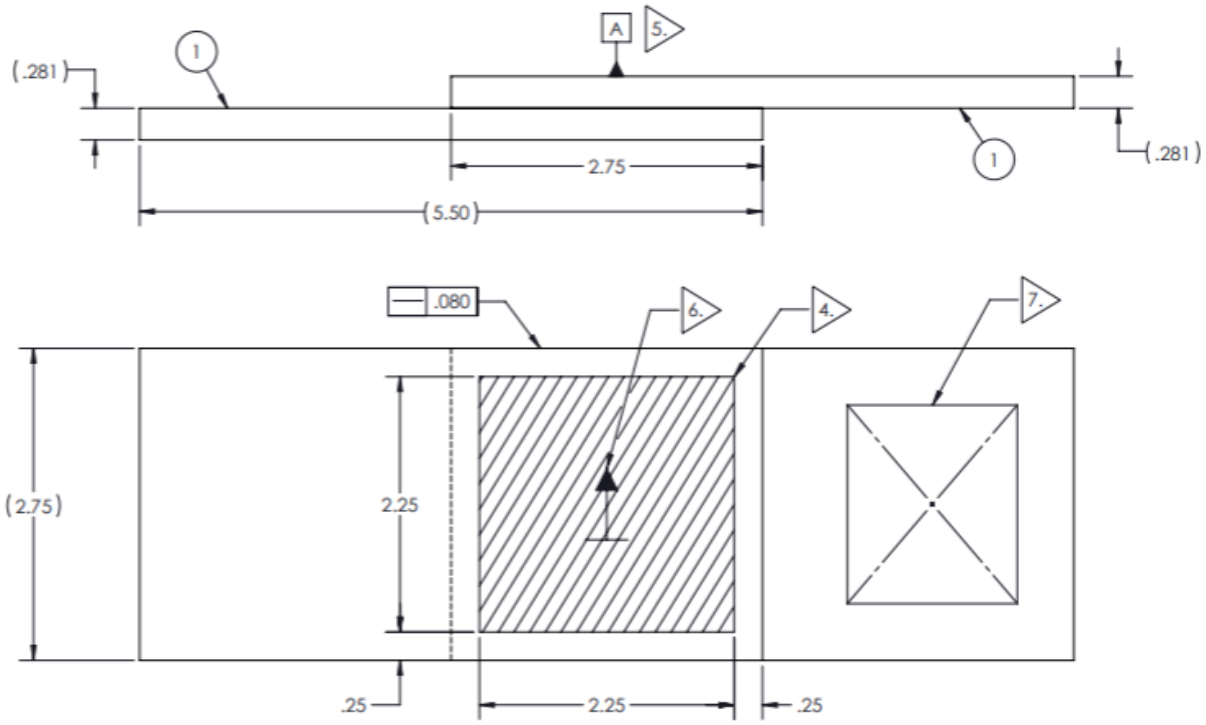


Figure 13. Weld setback specimen configuration, excerpt from drawing TDEA-275. Item 4 identifies the 2.25 in. x 2.25 in. target weld area. All dimensions are in inches.

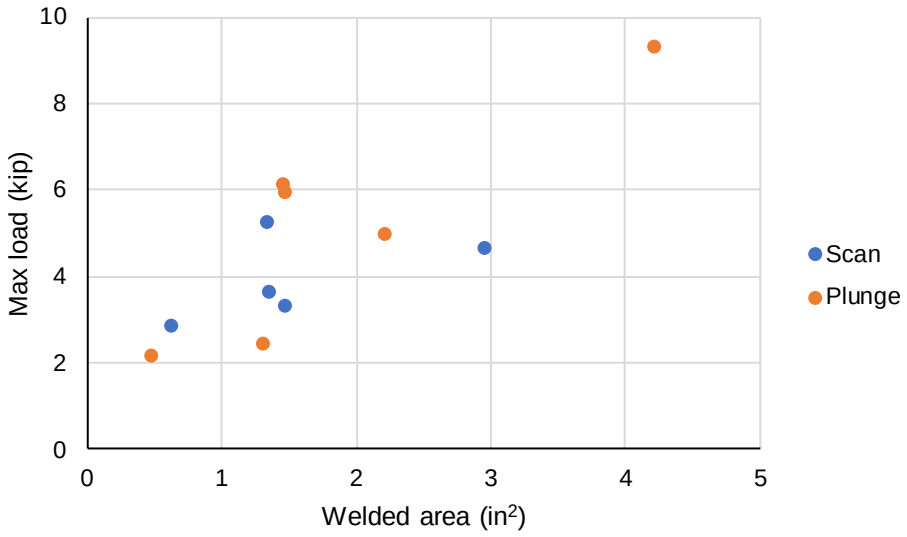


Figure 14. Weld setback test results.

In summary, the effort to scale up ultrasonic welding for the TSPD sub-element welding application uncovered numerous challenges related to lack of understanding and capability. A fundamental challenge is that the ultrasonic welding process is a highly transient thermomechanical process that relies on friction, which can be influenced by a wide variety of factors that may be difficult to control (e.g., surface condition, alignment, fiber/matrix distribution, voids). Conventional EDs with molded surface features (e.g., pyramids or holes) mitigate many of these challenges [20] and should be considered in future work to avoid the complications encountered here. Furthermore, measurement of temperature during welding was largely out-of-scope for this effort but appears to be a worthwhile avenue for future work since the post-test failure surfaces suggest underheating and overheating may have contributed to the welding challenges. Temperature data also supports process modeling, which can help explain the role of various process parameters. Finally, the welding trials demonstrated the risk of TPC welding producing unexpectedly weak bonds. As with thermoset adhesive bonding, some combination of process controls, witness coupons, proof loading, advanced NDE, or redundant load paths should be considered to address the potential for weak bonds. Despite the challenges, the TDEA team moved forward with an ultrasonic welding approach for the TSPD sub-elements, as summarized in Section 5.

# 3 Welding Methods: Summary of Advantages, Limitations, and Gaps

The resistance, induction, and ultrasonic welding methods assessed in the TDEA project show several advantages despite some limitations and development needs, as summarized in Table 2. The advantages and limitations in Table 2 are focused on the specific weld setups investigated in TDEA. Some general comments about the advantages and limitations of all the weld methods compared with adhesive bonding are provided as well.

Overall, an observation common to all three weld methods is that well-controlled pressure and temperature history are essential to produce a strong, well-consolidated weld. However, desired pressure and temperature histories can be difficult to obtain. The three weld methods are controlled with closed-loop schemes for a temperature proxy (current, amplitude, etc.), but cannot directly control weld-interface temperature. Closed-loop control for temperature and pressure may help improve weld outcomes but have not yet been implemented. Such a control scheme is complicated by the need for temperature sensing at or near the weld. While closed-loop pressure control may appear relatively easy to implement, it is important to recognize that the heated region should be held under pressure until

temperature cools below the glass transition temperature ($T_g$), which may require creative tooling concepts to be practical. In addition to these common challenges, each weld method has its own unique characteristics.

Resistance welding has the primary advantage of heat being applied directly at the weld interface, making it relatively insensitive to substrate thickness and layup. During resistance welding, the electrical resistance of the heating element can be monitored, and deviations potentially indicate an unsuccessful weld. Some limitations associated with resistance welding are related to the heating element itself. A carbon fiber heating element is desirable to avoid introduction of different materials in the joint, however, carbon fiber heating elements yield more variability in heating compared with metallic heating elements. Once the polymer melts, contact between the heating element fibers and substrate fibers creates alternative electrical paths and the "current leakage" phenomenon which interferes with heating at the interface. Current leakage makes it difficult to scale-up much beyond 1 $in^2$ weld areas. However, sequential welding approaches can mitigate this limitation. Future development could include novel electrically insulated heating elements that produce uniform heating and can be pre-integrated into one of the substrate faying surfaces to simplify assembly. The power used for resistance welds was relatively modest, probably because the process was longer and the heating more localized compared with the other welding methods. Peak power for the weldability study welds was 250 watts, and the average power was 120 watts over the 7.5-minute-long welding process.

The primary advantage of induction welding is that it enables noncontact heating. Assuming the HAZ is localized such that the surrounding unmelted material prevents deconsolidation, the pressure requirement can be lower than for other weld methods. In the work performed in TDEA, challenges arose with controlling the heating, especially near the edges of the specimens. The behavior of eddy currents near the specimen edges is a challenge. Heating well away from the target region can occur also. A related challenge is that the coil design may need to be updated for each welding application, which adds development time. The challenges encountered with welding the 0°-biased DCB specimens highlight the importance of layup in induction welding. Induction welding where the substrates are the susceptors may impose stringent limitations on the substrate layup to ensure adequate heating. It is also noteworthy that induction heating is sensitive to the fiber material properties and additional challenges may arise in applying induction welding to high-modulus fibers due to differences in their thermal and electrical properties. Future developments with induction welding should work toward establishing procedures for effective and controlled heating near geometric features and with common composite layups. In the induction welds performed for the weldability study with adherends having AS4 fibers, the power required was 500–1000 watts. Active cooling of the induction coil may be required, which would add to the power requirement.

Ultrasonic welding is very fast and applies heating and pressure in the same operation. Conventional ultrasonic welding uses an ED having molded pyramids or holes (i.e., mesh). Ultrasonic welding has been proposed with a "flat" ED, in other words, a resin film with no additional preparation [22] and no ED [23]. Agile Ultrasonics, in their work for TDEA, started with no ED and in later iterations used a flat ED. NIAR recently reported data suggesting it is difficult to obtain high LSS with low COV without the use of a traditional ED [24]. Since the heat generation is due to friction, small differences in alignment, pressure distribution, and surface roughness (and flatness) play an obvious role in nonuniform heating. These factors likely need to be controlled for successful weld operations. Internal features of the material (e.g., fiber distribution, porosity) are also important since viscoelastic heating is significant. Substrate thickness, layup, porosity, and fiber volume fraction variability may all need to be accounted for in process parameters. Both NIAR and Agile Ultrasonics required numerous iterative process trials to obtain a suitable set of weld process parameters, so future work should aim to reduce the recipe-development burden. Closed-loop temperature control may be helpful in this regard. A challenge unique to ultrasonic welding is to address joint tolerances and misfit surfaces. Since the sonotrode force is a parameter relevant to both heating and pressure, it may be difficult to decouple the heating from the applied pressure. During the TDEA project, several different configurations of ultrasonic welding were explored, each with differing power requirements. For 16-ply QI adherends welded in the standard SLS configuration, a low amplitude, longer duration process had a modest power requirement of about 250 watts (average). In contrast, high amplitude, short duration welds used about 1600 watts average with peak readings around 2000 watts. These power levels do not include heated tooling or sonotrode translation (for scan welds).

Table 2. Advantages, limitations, and needed developments for three weld methods.

| | Resistance | Induction | Ultrasonic |
|---|---|---|---|
| Advantages | • Heating applied at substrate interface, independent of substrate thickness, layup<br>• Monitor resistance for process feedback | • No additional materials at interface<br>• Rapid<br>• Potential for limited tooling<br>• Heating can be directed to substrate interface | • Rapid<br>• Pressure and heat application using the same system<br>• Potential for no additional materials at interface |
| Limitations | • Heating can be nonuniform<br>• Current leakage into conductive carbon fibers in substrate<br>• Electrical interference with thermocouples<br>• Added mass (heating element) | • Difficult to control heating, especially near edges, corners<br>• Heating sensitive to substrate thickness, layup, and boundary conditions<br>• Coil design may be application-specific<br>• Sensitive to fiber type | • Difficult to control heating, sensitive to alignment<br>• Resin film “energy director” may be required for quality and repeatability<br>• Heating sensitive to substrate thickness, layup, and surface and boundary conditions<br>• Propensity for fiber misalignment |
| In-Space Applicability | • Resistive heating element pre-integrated into adherend highly desirable to reduce part count<br>• Heating element trimming post-weld adds complication<br>• Power ($1in^2$ weld): 250 watts peak, 120 watts average, 7.5 minute duration | • Influence of electromagnetic field on nearby equipment must be managed<br>• Power ($1in^2$ weld): 500–1000 watts average, 40–60 second duration | • Energy director pre-integrated into adherend highly desirable<br>• Adherend alignment and fixture rigidity may be challenging to achieve<br>• Power ($1in.^2$ weld): 250 watts for 30 seconds or 1000–2000 watts for 3 seconds |
| Needed developments | • Closed loop (T, P) control scheme for improved repeatability<br>• Electrically insulated, uniform carbon fiber heating elements<br>• Heating element pre-integration into substrate | • Closed loop (T, P) control scheme for improved repeatability<br>• Established procedures for welding near edges, corners, and ply drops<br>• Methods to address heating challenges on 0°-dominated layups<br>• Application to adherends with high-stiffness fibers | • Closed loop (T, P) control scheme for improved repeatability<br>• Self-alignment<br>• Procedures for recipe development with fewer iterations<br>• Energy director and control schemes that can weld over misfit surfaces<br>• Application to high-stiffness fiber adherends |

Compared with adhesive bonding, welding has minimal surface preparation requirements [24]. However, TDEA found relatively high variability (high COVs), which suggests carefully developed and well controlled processing are required for successful welding (as is required for adhesive bonding). Since welds fuse the adherends, the complications associated with material interfaces in adhesive bonding and surface preparation are avoided. On the other hand, while bonding is a process localized to the adherend interface[2], welding produces a heat affected zone (HAZ) with size controlled by the applied thermal history. Improper thermal history or lack of consolidation pressure in the HAZ can lead to substrate degradation well beyond the interface region. Weld data reported in the literature surpasses maximum strengths possible with adhesive bonding, but TDEA did not reproduce this result. Further effort is needed to achieve such high LSS with low COV for relevant configurations. Additionally, an understanding of the LSS dependence on weld parameters is important. The above observations and recommendations are based on welding trials in a lab environment. As more data become available for welding in a simulated space environment, the development needs may change.

TDEA initially planned an assessment of conduction welding but later dropped it due the project descope. In conduction welding a heated rigid material is pressed against the outer surface of the adherend, thereby conducting heat through the adherend to the weld interface. Conduction welding looks appealing for potential ease of temperature and pressure control compared with resistance, induction, or ultrasonic welding, but may be limited to relatively thin parts and require more extensive tooling and higher power. Conduction welding is recommended for future evaluation.

# 4 Evidence of In-Space Welding Applicability

Welding for in-space assembly represents a first step toward the longstanding vision of in-space manufacturing of large structures enabled by TPC. No significant impediments to in-space application of TPC welding have been identified. However, several space environmental factors have not yet been adequately addressed. The primary environmental factors that need to be addressed to assess the potential for in-space welding as identified by TDEA are: 1) vacuum environment, 2) cold temperature environment, 3) sensitivity to contamination (for on-surface welding), and 4) outgassing. TDEA had plans to acquire test data regarding these four factors. As a result of project descope, TDEA only addressed contamination and partially addressed outgassing. Development of space-rated welding equipment is also needed but is considered herein as future work.

This section includes a summary of data obtained in TDEA and other recent NASA efforts that address the applicability of TPC to space environments and space structure applications. Additionally, the data include material property data relevant to space environments, welding trials with lunar regolith simulant contamination, and reassembly trials. The ability to disassemble and reassemble joints is not strictly required for in-space welding applications. However, it is viewed as a high-priority capability since it addresses the goal of developing reconfigurable and repairable in-space structures for long-term applications.

## 4.1 Material property data relevant to space environments

High-performance TPCs have flight heritage in low earth orbit (LEO) applications. PEI reinforced with aramid fiber was used for the webs on the AstroMesh® reflector on the Soil Moisture Active/Passive (SMAP) mission [25]. These TPC webs were welded together to support the reflector mesh. IM7/PEEK tubes comprise the Canadarm2 structure on the International Space Station (ISS) [26]. Some material property data have been reported (e.g., [27, 28]), however the public database of TPC material properties for space structure design remains relatively sparse. Some recent NASA-led efforts to fill in the TPC material property database by the authors and collaborators are summarized in the remainder of this section.

[2] It is noted that bonding is theoretically a process localized to the adherend interface while in practice an elevated temperature cure cycle is often applied by heating the region or entire part, which can introduce additional challenges.

The TDEA project conducted measurements of outgassing and coefficient of thermal expansion (CTE). Outgassing measurements were made following ASTM E595 [29] using unidirectional specimens manufactured from four materials: AS4/PPS, AS4/PEEK, AS4/PEI, and T700/LM-PAEK. Three replicates were tested for each material. Additionally, tests were also conducted for a piece of T700/LM-PAEK prepreg (prior to applying a processing cycle). The test results are summarized in Table 3. Typical requirements for spacecraft are CVCM < 0.1% and TML < 1.0%, which is satisfied for all materials evaluated. It is noted that these tests were run at 257 °F, which is below the $T_g$ for these materials, and additional off-gassing may occur at higher temperatures. Outgassing certainly occurs when temperature exceeds the processing temperature range, and the polymer starts degrading. Direct characterization of outgassing at processing temperatures is needed future work.

As part of the Polymer Aerogel and Composites Experiment (PACE) on MISSE-20, characterization of exposure to atomic oxygen is being conducted. Previously, 3D printed PEI and PEKK were evaluated via MISSE and found at most a small change in mechanical properties after exposure [30].

CTE measurements were performed following ASTM E289-17 [31] for AS4/PEEK and T700/LM-PAEK. Unidirectional 6 in. x 2 in. x 0.1 in. specimens were cut from panels manufactured in a heated press. Thermal expansion was measured from −275 °F to 120 °F at 1.8 °F/min (1 °C/min). Two replicates were measured in the fiber direction and four replicates were measured in the transverse direction. The thermal expansion as a function of temperature data was recorded. The CTE averaged over −275 °F to 68 °F is summarized in Table 4.

Table 3. TDEA outgassing test results (ASTM E595).

| Material | Total mass loss (TML) | Water vapor regained (WVR) | Collected volatile condensable materials (CVCM) |
|---|---|---|---|
| AS4/PPS | 0.03% | 0.01% | 0.00% |
| AS4/PEEK | 0.07% | 0.06% | 0.00% |
| AS4/PEI | 0.13% | 0.11% | 0.00% |
| T700/LM-PAEK | 0.10% | 0.06% | 0.00% |
| T700/LM-PAEK prepreg | 0.09% | 0.06% | 0.01% |

Table 4. TDEA CTE test results, −275 °F to 68 °F .

| Configuration | Average CTE [ppm/K] |
|---|---|
| AS4/PEEK, 0° | 0.82 |
| AS4/PEEK, 90° | 27.6 |
| T700/LM-PAEK, 0° | 0.47 |
| T700/LM-PAEK, 90° | 28.0 |

Table 5. Summary of coupon tests evaluated at room temperature and cold temperature (n=6).

| Label | Description | ASTM Standard | Layup | Dimensions (in.) |
|---|---|---|---|---|
| 0T | Lamina Tension | D3039 | $[0]_6$ | 10.0 x 0.5 |
| 90T | Lamina Tension | D3039 | $[90]_8$ | 7.0 x 1.0 |
| 0C | Lamina Compression | D6641 | $[0]_{14}$ | 5.50 x 0.5 |
| 90C | Lamina Compression | D6641 | $[90]_{14}$ | 5.50 x 0.5 |
| IPS | In-plane Shear | D3518 | $[+45/–45]_{4s}$ | 10.0 x 1.0 |
| UNT | Unnotched Laminate Tension | D3039 | $[45/0/–45/90]_{2s}$ | 10.0 x 1.0 |
| UNC | Unnotched Laminate Compression | D6641 | $[45/0/–45/90]_{3s}$ | 5.50 x 0.5 |
| OHT | Open Hole Tension | D5766 | $[45/0/–45/90]_{2s}$ | 12.0 x 1.5 |
| OHC | Open Hole Compression | D6484 | $[45/0/–45/90]_{3s}$ | 12.0 x 1.5 |

The Cryotank Technology for Exploration Applications project characterized TC1225 (T1100/LM-PAEK) mechanical properties at room temperature, $-150°F$, and $-320°F$ with ambient moisture conditions. Specimens were cut from press-consolidated panels consolidated per the National Center for Advanced Materials Performance (NCAMP) processing specification for TC1225. The test configurations, applicable ASTM standards, layups and dimensions are summarized in Table 5. The cold-temperature mechanical property results are normalized with the room-temperature data and summarized in Figure 15. In terms of strengths, the compressive properties (0C, 90C, UNC, and OHC) show an increase at cold temperatures, whereas the tensile (0T, 90T, UNT, and OHT) and shear (IPS) properties decrease, especially at $-320°F$. The changes in modulus are less pronounced than for strength. However, the matrix dominated test results (90T, 90C, and IPS) show modest increases at cold temperature. In summary, there is some temperature dependence to the mechanical properties of TPCs. However, for the cases where there are property knockdowns (e.g. 90T strength), the knockdowns can be addressed with design and sizing considerations.

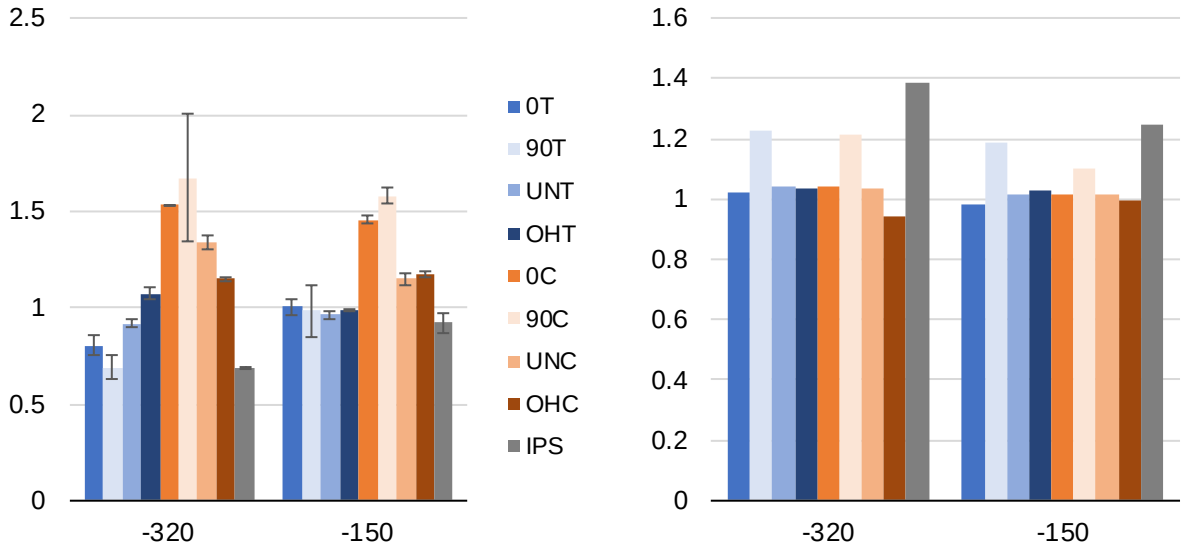


(a) Normalized strength (ksi) at –320 °F and –150 °F

(a) Normalized modulus (Msi) at –320 °F and –150 °F

Figure 15. Summary of mechanical property data normalized with room temperature ambient values. The strength error bars show one standard deviation.

Finally, mode II fracture toughness was measured at room temperature and in liquid nitrogen (–196 °C) for a variety of TSC and TPC materials [32]. The preliminary results show the TPC materials have about 400% higher cryogenic toughness than the TSC materials. It is also noteworthy that the TPC cryogenic mode II fracture toughness is higher than room temperature toughness of the TSC materials. This result suggests that damage tolerance and microcracking challenges common with TSCs may be substantially mitigated with TPCs.

## 4.2 Ultrasonic welding trials with lunar regolith simulant contamination

Contamination is relevant for welding on dusty planetary surfaces. Thermoplastic composite welds are known to be more resilient to contamination than adhesive bonding [24]. TDEA conducted tests to evaluate LSS knockdowns with lunar regolith simulant LHS-1 [33] introduced at the weld interface. Ultrasonic welding was used with 16-ply QI TC1225 substrates with and without one layer of a 0.0024-in.-thick LM-PAEK film. No data was available to inform relevant amounts of dust contamination, so two levels were considered and denoted “low” and “high”, as shown in Figure 16. The low dust level is between $2.82 \times 10^{-5}$ oz/in$^2$ and $1.13 \times 10^{-4}$ oz/in$^2$. The high dust level is between $1.55 \times 10^{-3}$ oz/in$^2$ and $1.98 \times 10^{-3}$ oz/in$^2$. These dust levels indicate the condition after dust was deposited on the adherends, prior to welding. The LSS results are shown in Figure 16 and indicate no knockdown for “low” dust concentration. There is potentially a small knockdown for “high” dust concentration without film. The dust may act as an energy director during welding or a particulate reinforcement. It is also possible that the ultrasonic vibrations evacuated most of the dust prior to adherend melting. One caveat with this data is the ultrasonic weld recipe used generates defects (as discussed above) and does not generate the expected LSS associated with a well consolidated joint in the baseline (no dust) condition. The knockdowns may be different for a different weld process. Future work is needed for a more thorough investigation of the effect of lunar dust contamination.

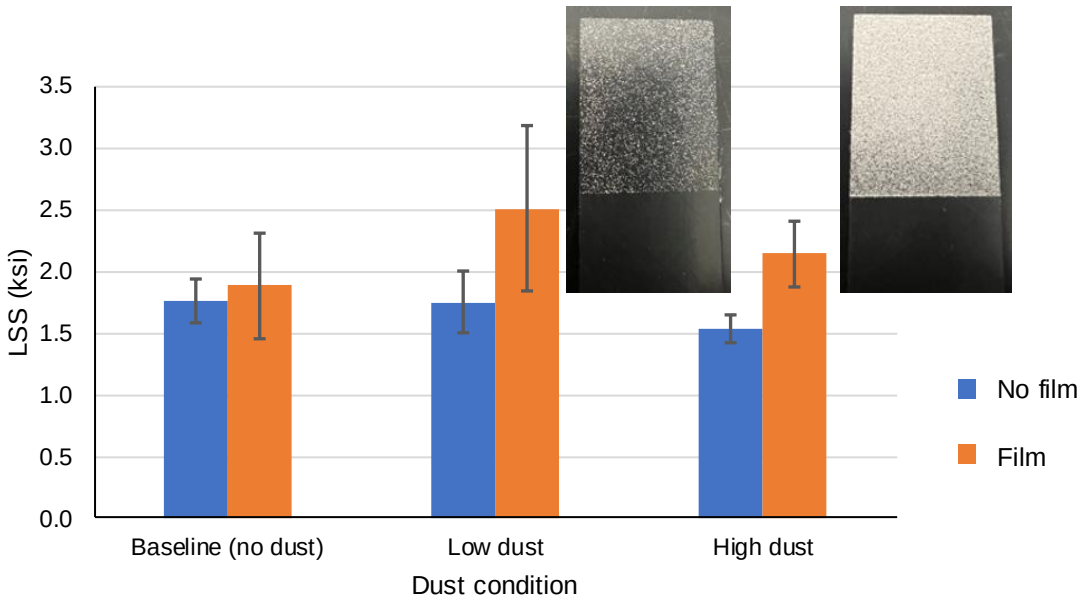


Figure 16. LSS from dust contamination testing. Error bars show one standard deviation for n=10. Blue bars (left) are specimens without a film interlayer, and orange bars (right) are specimens with an LM-PAEK film interlayer at the bonding surface. The inset photographs show an example of dust conditions after dust was applied to adherends, prior to welding.

## 4.3 Preliminary reassembly trial

Thermoplastic composites are reprocessable and that can be leveraged in a space manufacturing system to support sustainability and changing mission needs. A feasibility study was conducted at NASA Glenn Research Center to determine whether TPC adherends could be joined together using a dissimilar thermoplastic film, disassembled, and reassembled. A PEEK/carbon fiber QI panel was successfully joined using an LM-PAEK film interlayer using a hot press, Figure 17. SLS tests were completed with some tests at elevated temperatures, and the coupons were successfully reassembled using a custom frame and additional film interlayer. Other parameters investigated were film material, adherend material and layup, and film thickness. Strength data was collected and failure mode was recorded. It was concluded that reassembly of thermoplastic composites is feasible, but requires additional optimization such as reducing film squeeze out [34]. Relatively high loads were required to break the specimens even at elevated temperatures, and so disassembly was uncontrolled. In future work, alternative interlayer material and disassembly at higher temperatures should be investigated so that the interlayer material can be melted or significantly softened to allow controlled disassembly without deteriorating the adherends.

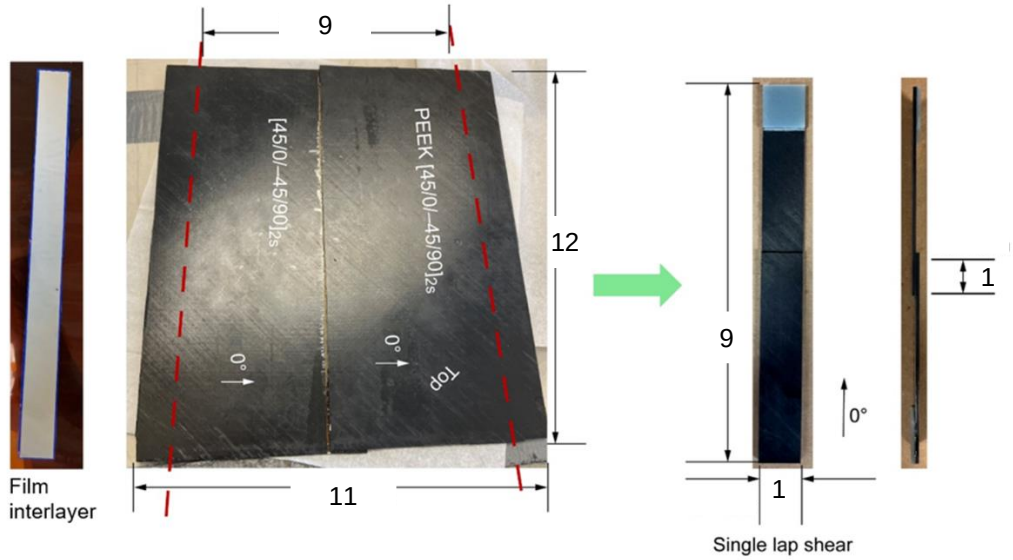


Figure 17. AS4/PEEK QI panel joined using a LM-PAEK film interlayer using a hot press. The panel was machined into 10 SLS coupons for mechanical testing and re-assembly trials. Dimensions in inches.

# 5 Structural Scale Joining: TSPD Subelements

The TDEA project developed a thermoplastic in-space point design (TSPD) to focus development efforts. The TSPD is a tower structure, as shown in Figure 18, that would be used to elevate vertically oriented solar arrays for near continuous solar illumination at the south-pole of the Moon. The 168-ft-tall tower uses a truss design with the assumption that truss elements will be fabricated on Earth and then delivered to the lunar south pole where they would be assembled via robotic manipulators and welding processes to erect the tower. The TSPD global design and analysis are described in [21]. Based on the TSPD global structure, a subelement test article, representing the most highly loaded joint was developed, manufactured, and tested. This section provides an overview of the manufacturing, welding, and performance assessment of the TSPD subelement structural test article. It is intended as a representative example of an application where in-space welding operations may eventually be deployed. The TSPD test article has relatively thick laminates (up to 0.3 in.) compared typical space structure laminate thicknesses.

The goal of the TSPD vertical subelement test effort was to advance ultrasonic welding toward future lunar surface assembly applications by manufacturing the TSPD vertical joint and characterizing its structural behavior. The objectives of the effort were: 1) build and test articles with the TSPD vertical joint geometry and with representative loading and scale, 2) develop an ultrasonic welding process for structural joining, 3) identify the as-manufactured condition via nondestructive inspection, 4) characterize the joint structural behavior via test, and 5) correlate the structural test with analysis results. Based on the TSPD global analysis, the design limit load (DLL) was established as 16.7 kips [21]. Considering the welded joint a discontinuity, the design factor for the joint is 2 DLL per reference [35]. While meeting this requirement was an element of the test effort, it was not formalized as a test objective because of the relative immaturity of the welding approach and challenges in producing strong defect-free welds encountered at the coupon scale. The remainder of this section describes the effort to design, analyze, manufacture, and evaluate the TSPD subelements.

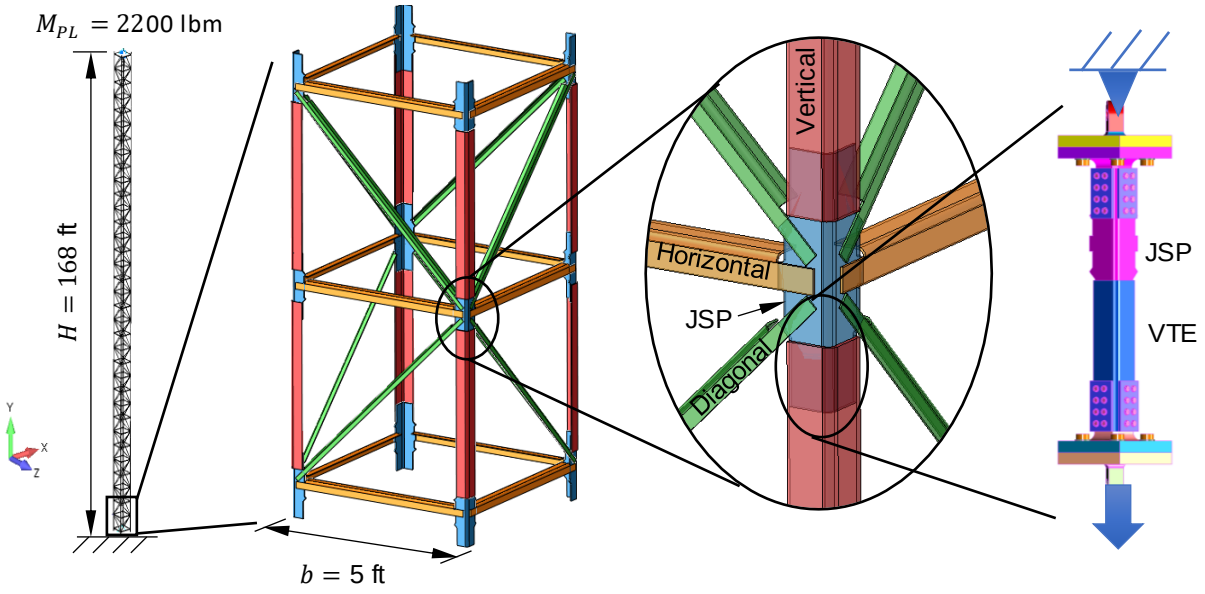


Figure 18. TDEA TSPD. The joint region is shown with transparency so that the overlap (welded) regions are visible. The TSPD subelement comprises a vertical truss element (VTE) and joint splice plate (JSP).

## 5.1 Subelement test article design

The subelement test article was designed to validate that the vertical joint under tension loading (other loading modes were not considered due to early termination of the project). The test article comprises a joint splice plate (JSP) with layup $[45/90/–45/0_{13}/45/90_2/–45/0_6]_s$ and a short vertical truss element (VTE) with layup $[(45/0_3/–45/0_2)_4/0_2]_s$, as shown in Figure 18d and Figure 19. The JSP and VTE are welded in two locations where the flanges overlap. The overlap length is 5.0 in. The 10.1 in.$^2$ weld area included ≥ 0.25-in. standoff from specimen edges and the corner region. Load introduction occurs through metallic end fixtures that located the load with a designated offset such that bending in the joint is relatively close to the joint load condition predicted in the global TSPD structural analysis. The end fixtures also included a pinned connection to prevent transferring moment into the test stand. The metallic end fixtures were connected to the weldment via bolted connections with a no-slip design condition (i.e., a friction joint). The test specimens are identified by TDEA-409-X where 'X' is a letter A-H identifying the test specimen replicate.

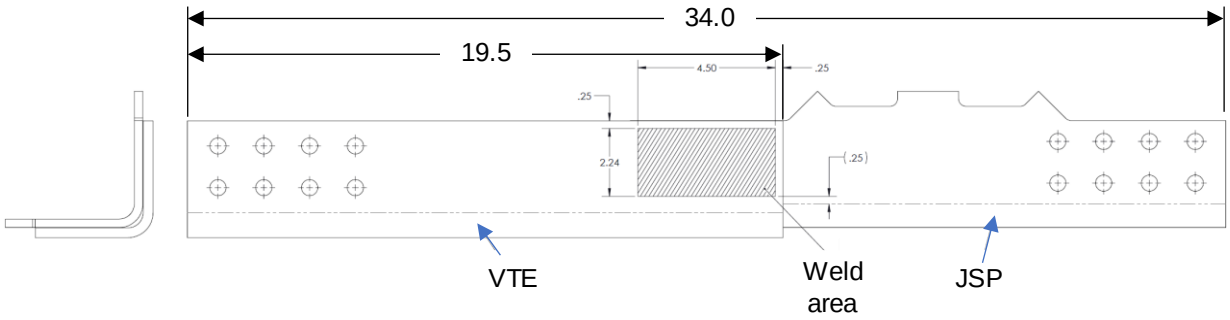


Figure 19. Subelement weldment geometry. Load introduction fixtures are not shown. All dimensions in inches.

## 5.2 Finite element model

A finite element (FE) model of the test article and end fittings was created, as shown in Figure 20. Most of the elements in the model are solid elements, and the typical element size is 0.2 x 0.2 in. The model was intended to not only assess the load carrying capacity and quality of the load introduction hardware, but also to simulate the entire test assembly behavior prior to tensile testing. The FE model was created in Femap [36] and was solved with geometric nonlinearity in MSC Marc Mentat [37]. The test article was modeled using solid elements with linear-elastic material properties. The welded interface was modeled with a uniform mesh and merged nodes and included the 0.25-in.setback around the perimeter of the welded area, which corresponded to the setback previously mentioned in section 2.5. The end fittings and lug portion of test fixtures were also included in detail where all bolts, washers, and preload with contact properties were defined and implemented.

A second model was created in Abaqus for the purpose of strength prediction. This model included a similar representation of the VTE and JSP but used a coarse representation of the boundary conditions with rigid constraints. The joint was modeled with a single layer of cohesive elements. Analyses were run with varying interface fracture toughness values, intended to be representative of different weld processes. Additional details are available in [21].

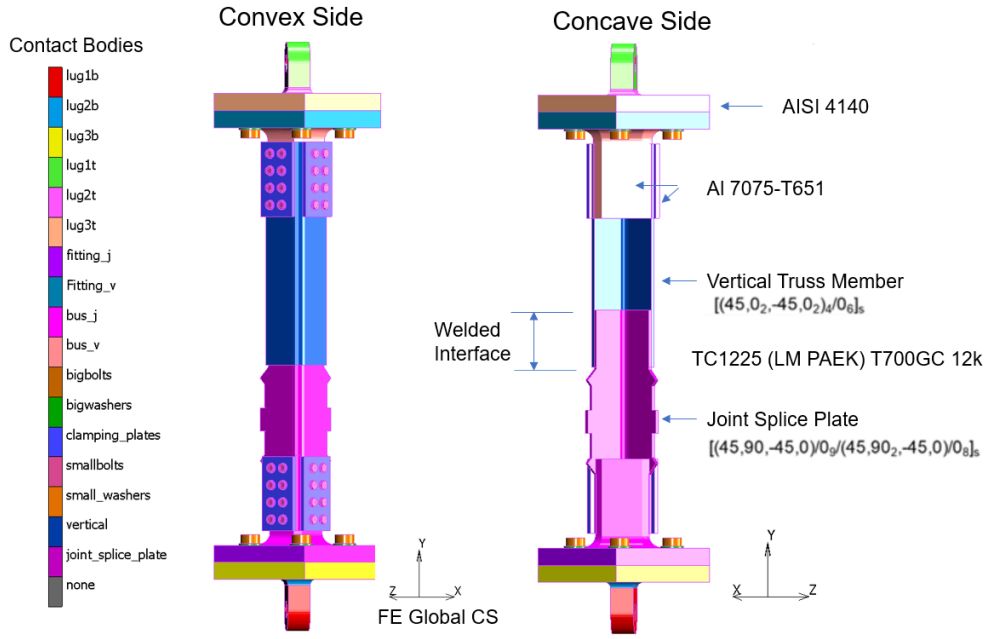


Figure 20. Pretest Marc model for the TSPD subelement test article.

## 5.3 Truss element manufacturing

Several VTE and JSP were fabricated from T700/LM-PAEK using an AFP system and consolidated using an autoclave at NIAR. Both parts have 'L' shaped cross-sectional profiles and so process induced deformation (i.e., spring-in) was nonnegligible. Adequate compensation for spring-in was identified as critical to achieving good fitment between the VTE, JSP, and load introduction hardware. An empirical spring-in correction was pursued wherein initial trial parts were made using the correct laminate ply design, at a 1/8$^{th}$ length scale on a tool with a 90° and 0.25-in.-radius corner. The spring-in angle was measured after the autoclave cycle for each part and then applied as tool compensation for subsequent parts. However, the lay down and consolidation quality in the corner region of the 'L' section changed prior to the final design, which had a 0.5 in. corner radius and a revised caul plate. As a result, the spring-in compensation was not ideal, with a resulting angle mismatch of 1.5 degrees between the VTE and JSP, as shown in Figure 21. In the case where the parts were aligned with equal gap on both legs, the maximum gap was 0.026 in.

Conversely, when one side of the joint was held flush forcing the gap to the other side, the maximum gap was 0.055 in. Due to the project schedule constraints, additional iterations to improve the part fit were not pursued. Instead, the welders were tasked with addressing the gap between the VTE and JSP, as described in the next section.

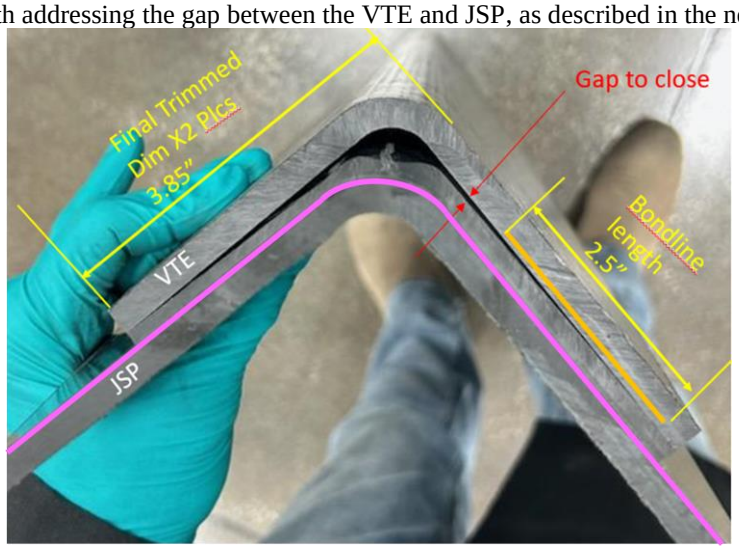


Figure 21. Photograph showing misfit between JSP and VTE due to part spring-in.

## 5.4 Subelement welding

Subelement test articles were welded by two different organizations using different ultrasonic welding approaches. Two specimens were welded at NIAR and six specimens were welded at Agile Ultrasonics. In all welds, the sonotrode was placed on the convex side of the VTE. For both organizations, the welding configuration was outside the realm of previous experience so the welds were treated as best-effort trials and the welding parameters were adjusted by the operators for each specimen. As a result of the challenges in achieving high LSS (Section 2), the emphasis in the subelement welding was to achieve the required joint strength. Hence, efforts to evaluate suitability for in-space welding operations in terms of environment, tool/fixture practicality, power, and robotic operation were minimal and viewed as future work.

Agile Ultrasonics used a plunge welding approach, wherein the sonotrode was held fixed while the ultrasonic vibrations were activated. After the end of the vibration cycle and a short dwell, the sonotrode was raised off the part and repositioned for the next weld. The plunge welds proceeded along the longitudinal direction until the 4.5-in. weld length was traversed. Three passes were used to complete one side of the weld on specimen A. Two passes were used to complete the remaining joints. Agile also made use of a heated tool (300–350°F) with several clamps, Figure 22a, which closed the gap between the VTE and JSP. The gap was equally distributed between the two legs of the 'L' section. Four layers of 60-µm-thick LM-PAEK film were placed at the weld interface prior to welding. Weld process parameters were manually adjusted so that there was evidence of heating through the thickness of both laminates and so that obvious signs of overheating (i.e. smoke) were minimized. The plunge welds used 800-1000 watts for 20–25-second-long welds. Agile welded specimens were designated A, B, E, F, G, and H. Specimens A and B had between 14 and 30 plunge welds on each side. The best outcome was obtained with 14 plunge welds per side so that was used for specimens E, F, G, and H.

NIAR completed one weld using a plunge welding approach and then used a continuous welding approach for the remaining welds. In the continuous welding approach, the sonotrode translates along the part while the ultrasonic vibration is activated. One challenge with continuous welding is applying adequate pressure during cool down in the wake of the sonotrode. NIAR used a roller system for this purpose, as shown in Figure 22b. NIAR did not use preheating or a heated tool and used a simple clamping approach. The parts were positioned so that there was no gap in the first weld, and then all of the gap was taken up in the second weld through sonotrode and clamping force. LM-PAEK film was molded onto the weld surface prior to welding to act as an energy director (inset image in Figure

22b). The first side of the joint was set flush and utilized a 0.008-in.-thick film, while additional film was used on the second side to act as shim between the two parts, filling the gap. NIAR welded specimens C and D. Representative photographs of one specimen welded by Agile Ultrasonics and one specimen welded by NIAR are shown in Figure 23. The plunge welds each used about 230 watts for 30 seconds. The scan welds used about 500 watts for 30 seconds (for the ultrasonic excitation, not including the power required to translate the sonotrode along the part).

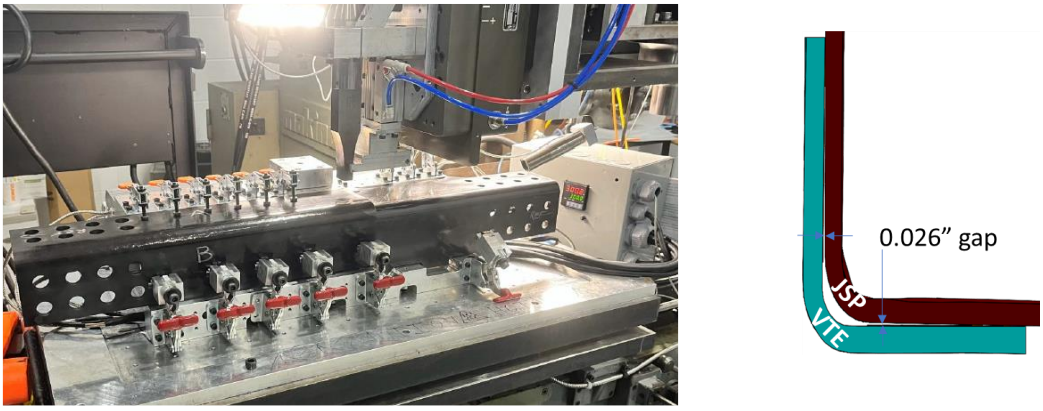


(a) Agile Ultrasonics weld setup


(b) NIAR weld setup

Figure 22. Welding setups used for the TSPD subelement. The schematics on the right show how the welding vendors positioned the VTE and JSP prior to welding.


(a) Agile Ultrasonics weld

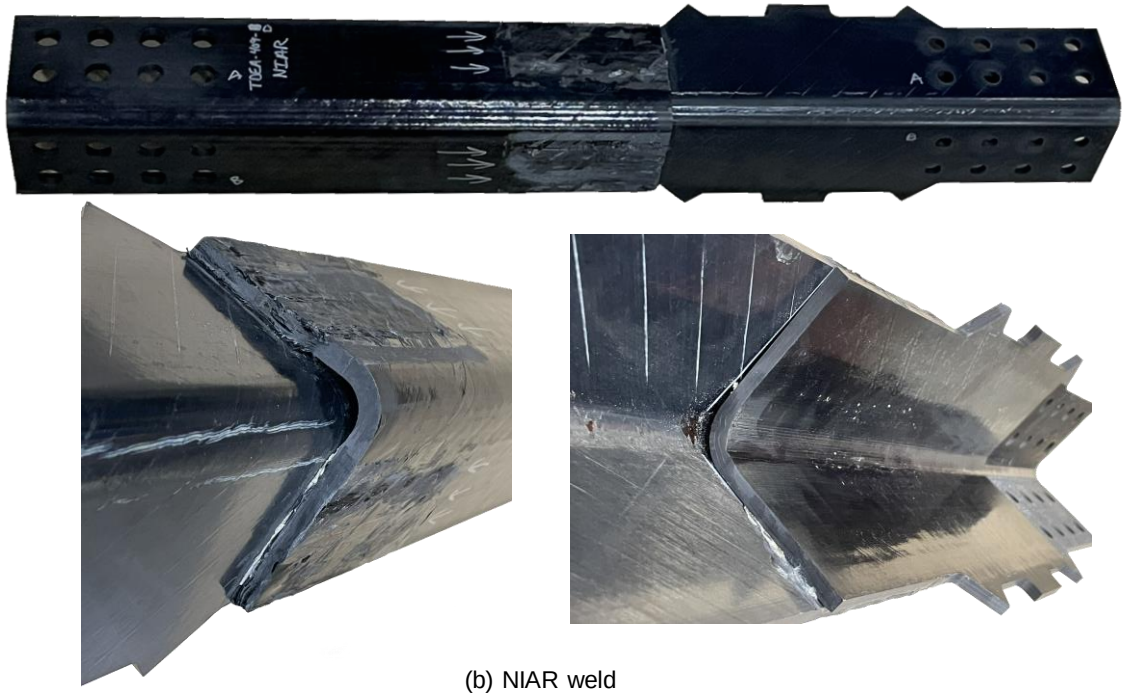


(b) NIAR weld

Figure 23. Photographs of (a) specimen B welded by Agile Ultrasonics and (b) specimen D welded by NIAR. In both designs blistering occurred on the sonotrode side and in the Agile weld also on the anvil side. Blistering was likely due to inadequate pressure or overheating. Fiber pushout is also evident at the end of the overlap.

## 5.5 Nondestructive inspection

Several of the specimens were inspected with X-ray computed tomography (XRCT) prior to testing. Defects were evident in all scans. In general, defects were more prevalent in the VTE laminate than the JSP laminate, perhaps because the sonotrode was in contact with the VTE[3]. Representative cross sections are shown in Figure 24, located around the middle of the overlap. Open delaminations were observed scattered throughout the weld area, often located within one or both truss member laminates (i.e., not necessarily at the weld interface). Regions with a darker shade of gray were also observed, indicating a lower density. These regions may have porosity with dimensions smaller than the scan resolution and therefore appear as lower density. Comparing the extent of defects through the thickness of the VTE and JSP, the Agile welds typically show evidence of defects in both the VTE and JSP. In contrast, the NIAR welds typically had more numerous and larger defects, but mostly contained within the VTE, with relatively few defects in the JSP. In Figure 24b, the right-hand side of the VTE displaced as evident by the nominal tangent to the corner shown with a yellow dashed line. This displaced position is probably due to the gap between the parts being positioned to one side the 'L' section.

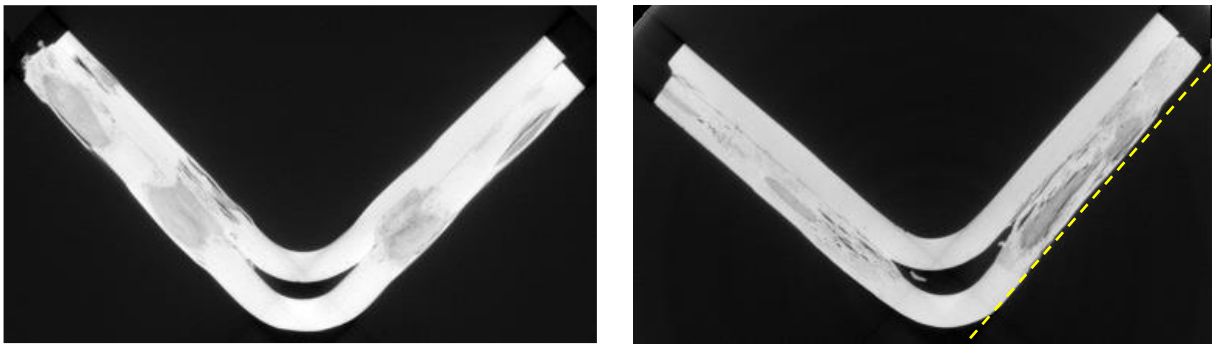

(a) TDEA-409-B (Agile) (b) TDEA-409-D (NIAR)

Figure 24. Representative XRCT slices located around the middle of the overlap. The yellow dashed line in (b) indicates a tangent to the corner at 90° from the other side.

## 5.6 Test setup and procedure

The test setup provided the capability to load the specimens quasi-statically to failure under tensile load while measuring load, strain, and displacement data. The measurements characterized the structural behavior of the vertical joint through failure. The test setup is shown in Figure 25. Analog data including load data, direct current displacement transformer (DCDT) data, and strain gage data were recorded at 100 Hz. Two digital image correlation (DIC) systems were utilized to capture full-field strain and displacement on the front and back sides of the test specimen at 1 Hz. The specimens were also monitored with standard and high-speed video on both sides. The specimens were loaded monotonically in displacement control at 0.005 in/min. Subcritical loading to 10%, 20%, and 50% DLL were conducted to ensure acceptable load introduction, alignment, and functionality of data acquisition systems. After completion of the 50% DLL subcritical loading, the specimens were unloading and then reloaded to catastrophic failure. Six specimens were tested, Specimens -A through -F.

[3] This is consistent with results from coupon welds, in which it was typically to observe more defects in the adherend that was in contact with the sonotrode as compared to the other adherend. See Figure 4 where the images for ultrasonic welding are arranged with the top adherend being the one that was in contact with the sonotrode.

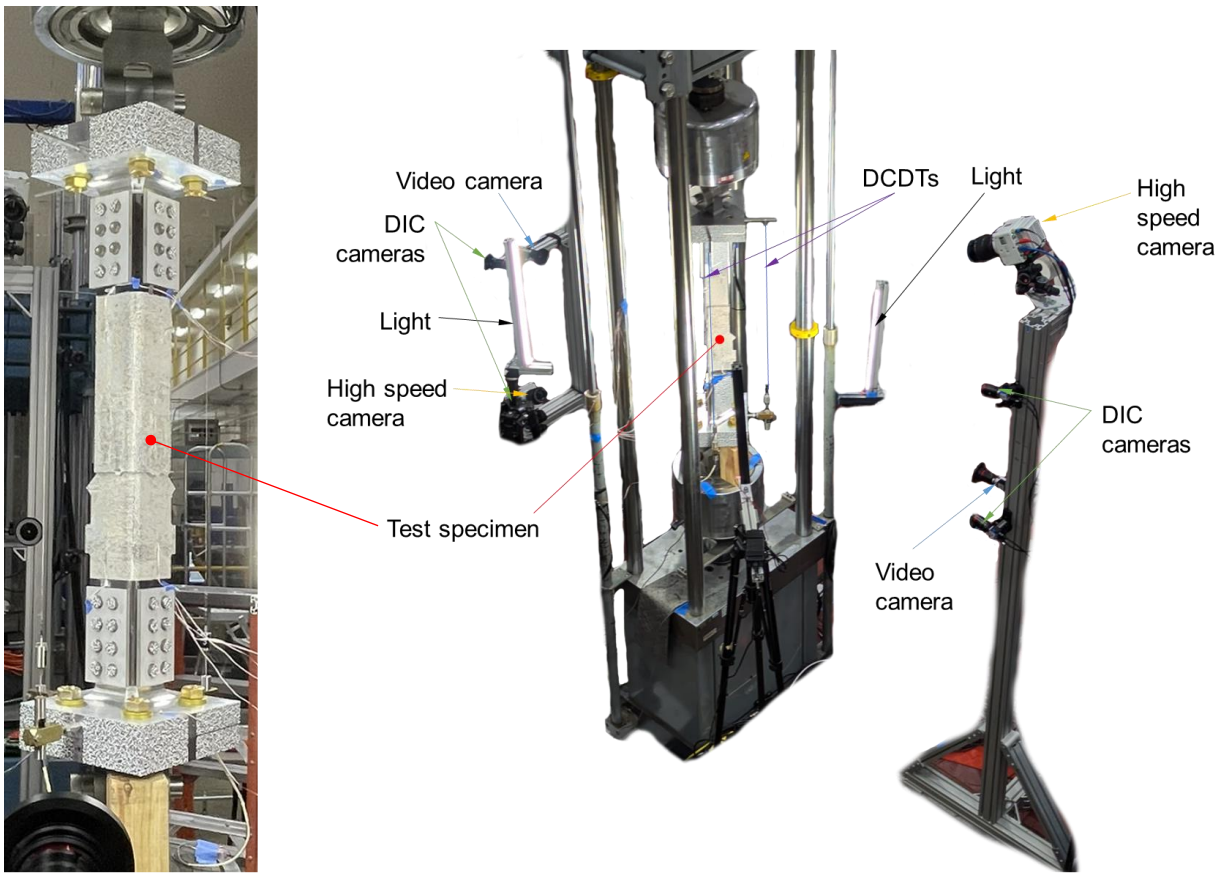

Figure 25. Test specimen installed in the test stand and test monitoring and instrumentation setup.

## 5.7 Test and analysis results

All six test specimens were loaded successfully to catastrophic failure. The average displacement from the three DCDT measuring the relative motion between the top and bottom aluminum end fixtures is plotted vs. load in Figure 26, showing the relative consistent response among the specimens and relatively good agreement with the pretest analysis results. There is some geometric nonlinearity, which is evident in both the test and analysis results. The test shows significantly more nonlinearity initially as load is first introduced. However, after about 0.005 in. of displacement, the slope of the test results and analysis matches very well. All six test specimens failed at loads exceeding 2x DLL. The failure event was abrupt and catastrophic. The average peak loads for the welds from NIAR and Agile Ultrasonics are 35.2 kips and 43.3 kips, respectively. Considering the four replicates welded by Agile, the CoV is 5.7%.

Prior to running these tests, efforts were made to predict the subelement strength, some of which are described in reference [21]. The models included a single layer of cohesive elements representing the welded connection between the VTE and JSP. With this modeling approach, the fracture toughness values for the cohesive elements are the critical parameters that control the predicted failure load. Efforts were made to calibrate the fracture toughness to the coupon scale weld data by manually tunning the value used in the analysis. However, due to the constantly changing welding process, variability in LSS, and the project schedule it was difficult to predict the strength with confidence. It is also noteworthy that these models ignore the defects observed in XRCT, and so it was unclear how those defects may influence the joint strength. The highest strength prediction corresponded to the case where the weld fracture toughness properties are equivalent to the interlaminar fracture toughness properties. The measured strength corresponds well with the prediction based on interlaminar fracture toughness properties, suggesting the weld toughness was around the toughness of the intrinsic material.

Among the TDEA test team, with mostly a background in thermoset composites, the numerous defects led to a perspective that the test article strengths would be relatively low. Therefore, the relatively high strengths achieved in the structural scale tests were surprising. It appears that these test articles were relatively insensitive to the observed defects. This could be a result of the particular loading configuration being relative benign with respect to the location and orientation of the defects. In other words, out-of-plane or fatigue loading may be much more sensitive to the defects. The relative insensitivity to the defects could also be explained by the much higher fracture toughness of the material compared with conventional thermoset resins. Further work is needed understand the effects of defects in welded TPC structures.

The correlation between the model and test results in axial strain field is shown with contour plots in Figure 27 for 2x DLL. The model results shown here are from post-test analysis using a 5.0% higher longitudinal modulus for the TC1225 material for improved agreement. Despite relatively low strains, the agreement is quite good both between test and analysis and among the test replicates. This result provides evidence that the model successfully captures the structural behavior of the joint.

The DIC data were used to obtain displacement across the joint to assess the structural behavior locally over the weld. Virtual extensometers were positioned on the convex side at 1.5 in. from the edge spanning 7 in. (1 in. beyond the overlap on both sides). The average virtual extensometer data are plotted against load in Figure 28, where the displacement data are smoothed with a 13-period moving average to help reduce the noise. The results show the specimens welded by Agile are slightly stiffer, perhaps due to better alignment associated with the more elaborate weld tooling. In all cases, some nonlinearity is evident in the structural response by around 30 kips. In several cases, audible damage events occurred and so the observed nonlinearity may be associated with subcritical damage propagation in the joints.

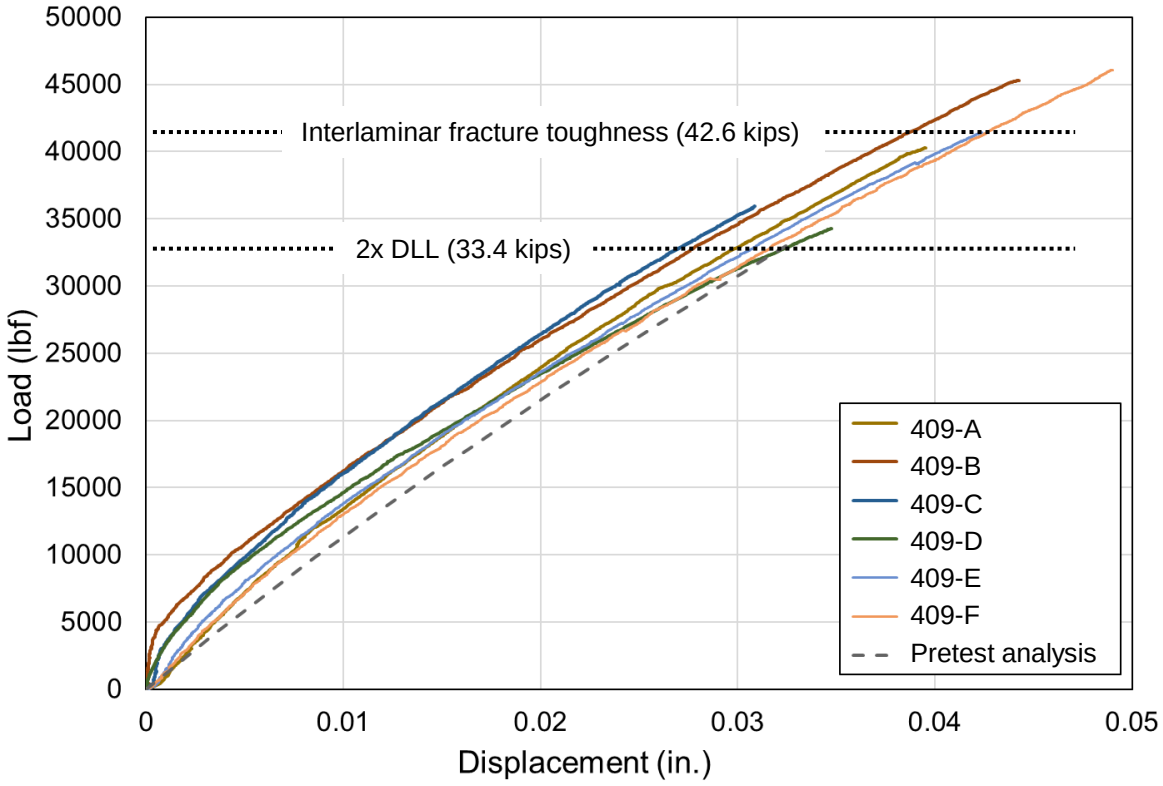


Figure 26. TSPD subelement load-displacement response. Test results are truncated at the point where catastrophic failure and abrupt load drop occurred.

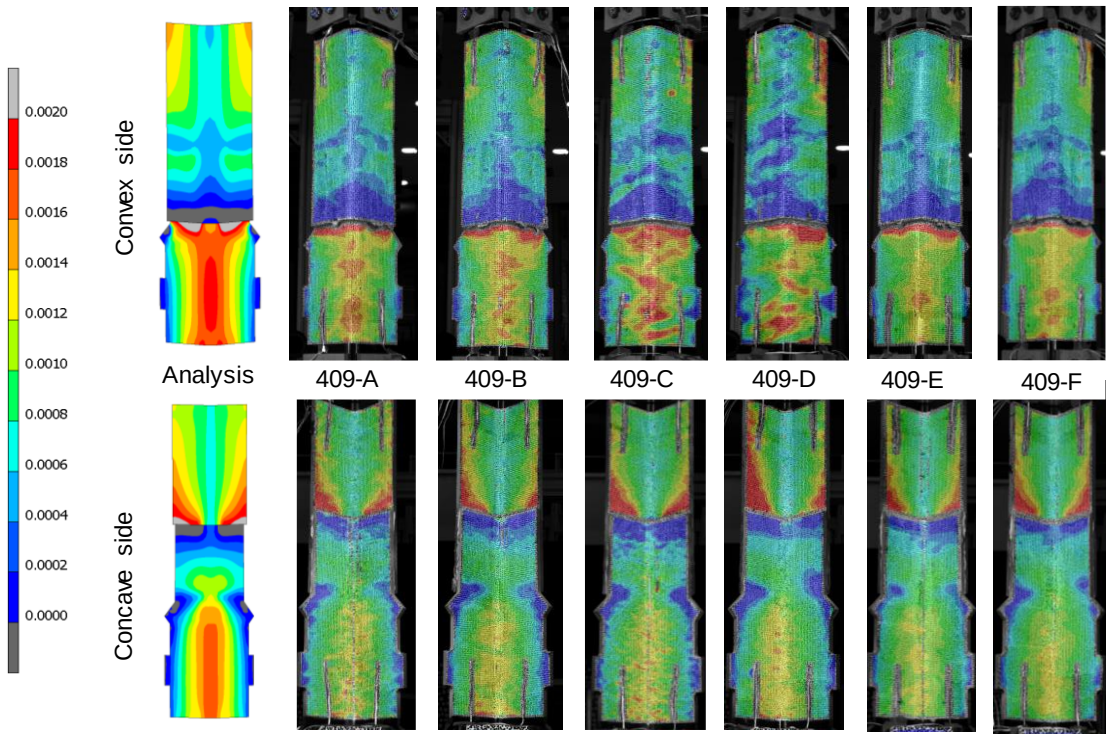


Figure 27. Axial strain contours from test and analysis results at 2x DLL.

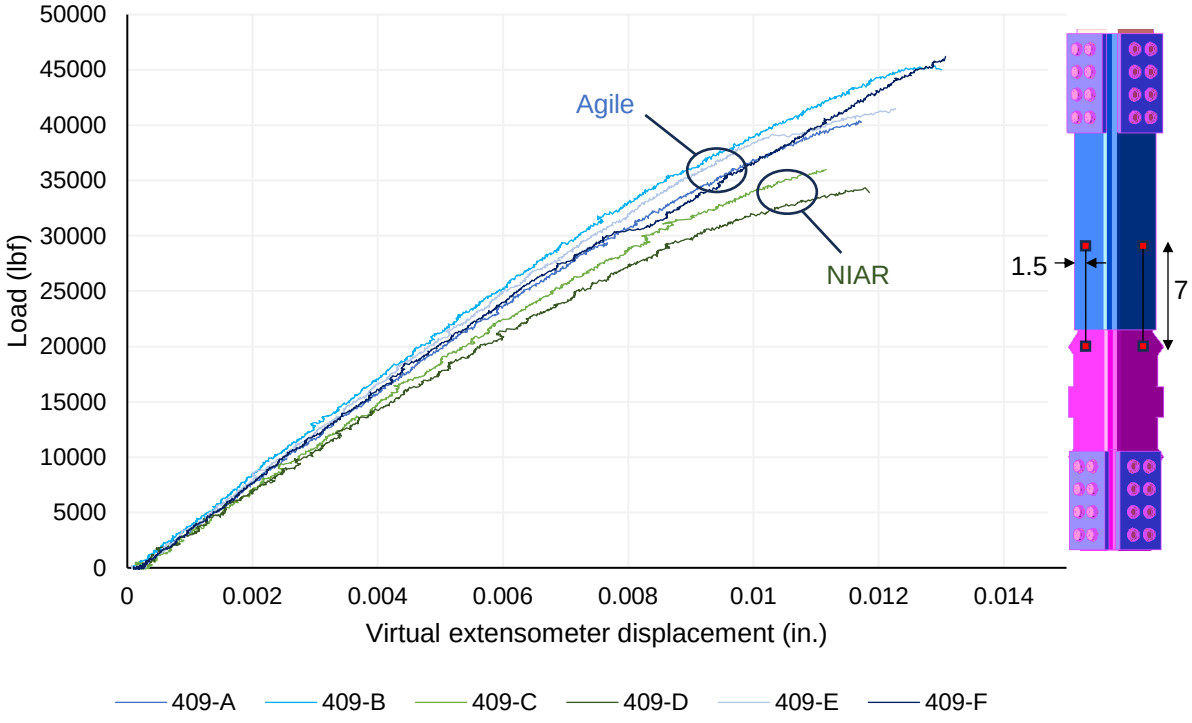


Figure 28. Average displacement across the joint, showing some nonlinearity starting at around 30 kips.

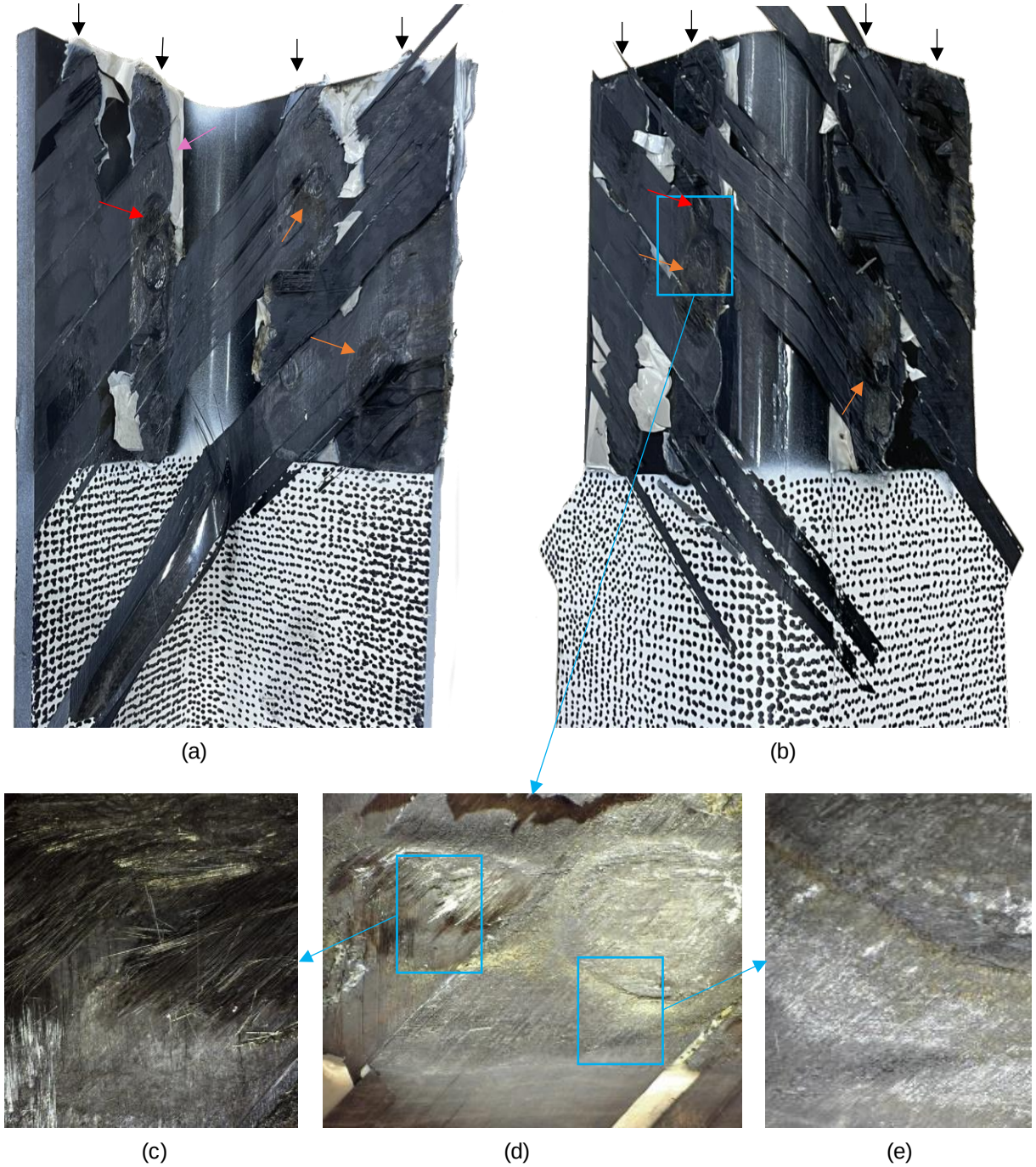


Figure 29. Photographs of failure surfaces, (a) and (b), from specimen B with close-up views in (c)–(e). The black arrows show the approximate location of the four passes of plunge welds. The pink arrow shows an example where the resin film did not melt. The orange arrows and (d) and (e) show locations where the resin is discolored yellow or brown, suggesting overheating and degradation. The red arrows and (c) show regions where the fibers were dry, suggesting the resin was significantly overheated and vaporized.

The failure surfaces showed similar characteristics across all six test specimens. Photographs of the failure surfaces of specimen B are shown in Figure 29. In general, the failure mode can be described as fiber tear as there is evidence of broken fibers and a few plies transferred from one adherend to the other. The failure surfaces also reveal some information about the welding process including regions that were underheated and overheated. The four passes of plunge welds are visible and contrast against regions where the material remained shinny and unwelded, and was observed near the edge of the welded part and also between the welding passes. The unmelted resin film also gives an indication of locations where the temperature remained relatively low, and no connection was made. The laminates for both parts have mostly zero-degree plies, and due to the orthotropic thermal properties, it is speculated that the heat may have spread out farther from the sonotrode along the axial direction compared with the transverse direction. This behavior is consistent with the regions where no weld was formed. The failure surfaces also give indications of overheating in the form of yellow or brown colored resin (orange arrows and (d) and (e) in Figure 29) and the absence of resin (red arrows and (c) in Figure 29). The brown resin was likely heated above the processing temperature range to the point of degradation. The regions with dry fibers (no resin) apparently experienced temperatures high enough to vaporize the resin. Therefore, these results suggest significant temperature gradients occurred during the welding process.

# 6 Concluding Remarks

Thermoplastic composite welding is a candidate for future in-space and on-surface structural joining applications. TDEA has contributed toward this long-term objective through hundreds of welding trials and evaluations. This report summarized the key findings from these welding trials. The findings are stated succinctly as follows:

1. Strong welds are possible as demonstrated at the coupon and subelement scale. Substantial process development effort is required to obtain this outcome for a particular weld method, material, and welding configuration, and to demonstrate repeatability. Though reasonably low COV were obtained for select weld configurations in this effort, repeatability remains a key challenge. The process development completed to date is insufficient for many configurations considered here. While thermoplastic composite welding has reached TRL 9 for some specific aeronautics applications and material systems (e.g., [17]), broad knowledge of these welding processes applied to space-application-relevant materials, environment, and configurations is still missing.
2. Defects, such as unwelded regions, delamination, porosity, burning, or distortion (thinning, fiber pushout) occurred for all weld methods and material combinations examined in TDEA to a lesser or greater extent as observed by NDE and verified by microscopy. The welds exhibit a heat affected zone that can extend beyond the target weld (overlap) region. These defects might be mitigated through better-controlled temperature and pressure histories during welding. Significant temperature history variation was observed in repeated nominally identical welding trials of resistance welding TC1200 (AS4/PEEK) at MSFC. The significant variability observed in the temperature history data may correlate with the variability in outcomes in terms of defects and strength.
3. Welding to the edge of relatively small specimens is a challenge, particularly for induction and ultrasonic welding where most previous application work focused on continuous welds with an emphasis on achieving good weld performance in the middle of a weld line (ignoring the start and stop regions). Ultrasonic welding up to edges is prone to create fiber push-out.
4. Ultrasonic welding of thick substrates and parts made by additive manufacturing is feasible, although the process needs to be tailored to the specific characteristics of the pieces being welded.
5. Ultrasonic welds of TC1225 (T700/LM-PAEK) show minimal sensitivity to lunar regolith simulant contamination.
6. Initial trials show evidence that reassembly of TPC welds is possible.
7. Structural-scale joining was demonstrated through a lap joint of L-section truss elements. The structural test data show relatively strong joints and a low 5.7% COV. The strength was in line with the predictions made using the interlaminar fracture toughness, which was surprising given large defects observed in the heat affected zone. This result was achieved after numerous iterations and is, counterintuitively, better than what

was achieved at the coupon scale. Applying the insights gained through the scale-up process to a new batch of coupon welds would be an interesting follow up.

Future work is needed to continue to mature thermoplastic composite welding technology toward in-space application. This report identifies several technology development needs following the TDEA effort, summarized as follows:

1. Weld technology developments in the lab environment:
    a. Introduce closed loop control for temperature and pressure or use other methods to reduce variability in applied temperature and pressure.
    b. Improvements to welding setup and tooling to achieve repeatable welds with minimal defects.
    c. Methods for substrate preparation for welding. Resistance welding: integrated and electrically isolated heating elements. Ultrasonic welding: integrated energy directors and alignment features.
    d. Models and process experience to relate process parameters to weld outcomes so that weld processes can be tailored to application requirements.
    e. Welding setups and test data for relevant space applications including adherend materials (e.g., high-modulus fibers) and configurations (e.g., tubes or deployable composites).
    f. Controlled methods of applying relevant thermal and pressure histories with short dwell times and high cooling rates to characterize material behavior in the heat affected zone.
    g. Correlation of thermal history to joint mechanical performance.
2. Weld processes trials and developments in space relevant environments:
    a. Weld trials in thermal vacuum chambers to prove relevant weld equipment operational capability, characterize weld outcomes, and understand welding system performance metrics and tradeoffs.
    b. Weld trials in microgravity (e.g., parabolic flights) to characterize lunar gravity or microgravity impact on polymer healing and welded joint material microstructure.

In summary, with substantial future work, thermoplastic composite welding may play a key role in large structures on future space exploration missions. At the same time, sustained investment in understanding the underlying physics of thermoplastic material and structural behavior improves the foundation for such application developments.

# 7 References


[1] J. T. Hoggatt and M. Kushner, "Applicability of thermoplastic composites for space structures," in *Langley Space Systems Technology Seminar*, Hampton, VA, 1978.

[2] M. L. Wilson, I. O. MacConochie and G. S. Johnson, "Potential for on-orbit manufacture of large space structures using the pultrusion process," NASA/TM 4016, Hampton, VA, 1987.

[3] NASA, "OSAM-1 On-Orbit Servicing, Assembly and Manufacturing-1," [Online]. Available: https://nexis.gsfc.nasa.gov/OSAM-1.html.

[4] NASA, "On-Orbit Servicing, Assembly, and Manufacturing 2 (OSAM-2)," 5 March 2021. [Online]. Available: https://www.nasa.gov/mission_pages/tdm/osam-2.html.

[5] L. M. Bowman, W. K. Belvin, E. E. Komendera, J. T. Dorsey and B. R. Doggett, "In-space assembly application and technology for NASA's future science observatory and platform missions," in *Space Telescopes and Instrumentation 2018: Optical, Infrared, and Millimeter Wave*, 2018.

[6] W. R. Doggett, J. Heppler, M. K. Mahlin, R. Pappa, J. Teter, K. Song, B. White, I. Wong and M. Mikulas, "Towers: Critical Initial Infrastructure for the Moon," in *AIAA SciTech Forum*, National Harbor, MD, 2023.

[7] J. R. Cooper, J. H. Neilan, M. K. Mahlin and L. M. White, "Assemblers: A Modular, Reconfigurable Manipulator for Autonomous in-Space Assembly," in *Ascend Conference*, Virtual, 2020.

[8] W. R. Doggett, J. Dorsey, T. Jones, M. Mikulas, J. Teter and D. Paddock, "TriTruss: A New and Novel Structural Concept Enabling Modular Space Telescopes and Space Platforms," in *70th International Astronautical Congress (IAC)*, Washington D.C., 2019.

[9] K. Song, O. Stohlman, B. White and R. S. Garatsa, "Structural Analysis, Modeling, and Testing of Multi-nut Joint for TriTruss Structure," in *AIAA SciTech Forum and Exposition*, Orlando, FL, 2025.

[10] J. L. Meyer, P. Lan, M. Bakir, I. Jasiuk and J. Economy, "Wide Area Reversible Adhesive for In-Space Assembly," *Macromolecular Materials and Engineering,* vol. 305, no. 7, p. 2000006, 2020.

[11] ASTM Standard D5868-01, "ASTM Standard D5868-01. Standard Test Method for Lap Shear Adhesion for Fiber Reinforced Plastic (FRP) Bonding," in *Annual Book of ASTM Standards*, ASTM Int., 2014.

[12] ASTM Standard D5528/D5528M-21, *Standard Test Method for Mode I Interlaminar Fracture Toughness of Unidirectional Fiber-Reinforced Polymer Matrix Composites,* West Conshohocken, PA: ASTM International, 2021.

[13] S. Miller, A. Bergan and e. al, "Assessment of Thermoplastic Composite Joining by Resistance, Induction, and Ultrasonic Welding," NASA/TM-20250006527, Cleveland, OH, 2025.

[14] W. Seneviratne, U. Palliyaguru, M. Walthers and A. Bleything, "An Assessment of the use of a Carbon Fiber Heating Element in Thermoplastic Resistance Welding for PEEK and PEI Thermoplastic Composite," NASA/CR-20250000834, Cleveland, OH, May 2023.

[15] W. Seneviratne, U. Palliyaguru and M. Walthers, "An assessment of the use of a Carbon Fiber Heating Element in Resistance Welding for PPS, PEI, LM-PAEK, and PEKK Thermoplastic Composite," Report 20250001324, June 2024.

[16] J. Fernandez, "Deployable Composite Boom (DCB) project," NASA Langley Research Center, https://techport.nasa.gov/projects/94176, Hampton, VA, 2021.

[17] J. W. van Ingen, A. Buitenhuis, M. van Wijngaarden and F. Simmons, "Development of the Gulfstream G650 induction welded thermoplastic elevators and rudder," in *Proceedings of the International SAMPE symposium and exhibition*, Seattle, WA, 2010.

[18] "ASTM Standard D3528. Standard Test Method for Strength Properties of Double Lap Shear Adhesive Joints by Tension Loading," in *ASTM Annual Book of Standards*, ASTM Int., 2016.

[19] I. Villegas and R. v. Moorleghem, "Ultrasonic welding of carbon/epoxy and carbon/PEEK composites through a PEI thermoplastic coupling layer," *Composites Part A: Applied Science and Manufacturing,* vol. 109, pp. 75-83, 2018.

[20] W. Seneviratne, J. Tomblin, M. Shafie, M. Walthers, A. Tummala, R. Ziegler and S. Tiwari, "Ultrasonic welding process development for thermoplastic aircraft fuselage skin panel," in *SAMPE Conference*, Long Beach, CA, 2024.

[21] A. C. Bergan and e. al., "Structural Analysis of a 50-m-Tall Thermoplastic Composite Truss Tower Structure for the Lunar South Pole," NASA/TM-20250001459, Hampton, VA, 2025.

[22] I. F. Villegas, "Strength development versus process data in ultrasonic welding of thermoplastic composites with flat energy directors and its application to the definition of optimum processing parameters," *Composites Part A: Applied Science and Manufacturing,* vol. 65, pp. 27-37, 2014.

[23] W. Tao, X. Su, H. Wang, Z. Zhang, H. Li and J. Chen, "Influence mechanism of welding time and energy director to the thermoplastic composite joints by ultrasonic welding," *Journal of Manufacturing Processes,* vol. 37, p. 196–202, 2019.

[24] W. Seneviratne, J. Tomblin, M. Shafie, M. Walthers, R. Ziegler, A. Tummala and S. Tiwari, "Thermoplastic Welding Process Qualification Protocols for Aircraft Design and Certification," in *FAA/JAMS Adhesive Bonding Working Group Meeting*, September 19, 2024.

[25] G. Gardiner, "Precision design for deployable space structures," *Composites World,* August 2016.

[26] A.-M. Lanouette, M.-J. Potvin, F. Martin, S. Mondor, D. Houle and D. Therriault, "Experimental Evaluation of the Canadarm2 Residual Flexural Strength After an Orbital Debris Impact," in *Proc of 13th European Conference on Spacecraft Structures, Materials & Environmental Testing*, Braunschweig, Germany, April 2014.

[27] J. Funk and G. Sykes, "The effects of simulated space environmental parameters on six commercially available composite materials," NASA TP 2906, Hampton, VA, 1989.

[28] D. M. Grogan, C. M. Ó. Brádaigh, J. P. McGarry and S. B. Leen, "Damage and permeability in tape-laid thermoplastic composite cryogenic tanks," *Composites Part A: Applied Science and Manufacturing,* vol. 78, p. 390–402, 2015.

[29] "ASTM Standard E595. Standard Test Method for Total Mass Loss and Collected Volatile Condensable Materials from Outgassing in a Vacuum Environment," in *Annual Book of ASTM Standards*, ASTM Int., 2021.

[30] M. M. Finckenor and J. R. McElderry, "Space Environmental Effects on Additively Manufactured Materials – Results from MISSE-9 and MISSE-10," 2023.

[31] "ASTM Standard E289. Standard Test Method for Linear Thermal Expansion of Rigid Solids with Interferometry," in *Annual Book of ASTM Standards*, ASTM Int., 2017.

[32] J. H. Kang, W. E. Flores and W. M. Johnston, "Overcoming Cryotank Challenges: Thermoplastic Resins Based on Integrated Computation and Experiment," NASA Langley Research Center, Center Innovation Fund, https://techport.nasa.gov/projects/146955, Hampton, VA, 2025.

[33] Space Resource Tech, "Lunar Highlands (LHS-1) High-Fidelity Regolith Simulant," 2024. [Online]. Available: https://spaceresourcetech.com/products/lhs-1-lunar-highlands-simulant.

[34] J. Pinakidis and S. Miller, "Joining, Disassembly, and Reconfiguration of Thermoplastic Composites for Space Applications," NASA/TM-20240002690, Cleveland, OH, May 2024.

[35] NASA Technical Standard, "Structural design and test factors of safety for spaceflight hardware, NASA-STD-5001B w/ change 3," 2022.

[36] Siemens AG, *Femap: Version 2023.*

[37] Hexagon, *MSC Marc Mentat, version 2024.2.*

# 8 Appendix A

Gaussian process regression (GPR) is a nonparametric, Bayesian approach for modeling complex and noisy data. In simple terms, GPR provides a flexible way to predict outcomes and quantify uncertainty by assuming that the data can be described by a continuous function. Instead of fitting a single curve, GPR employs a tunable covariance function, known as a kernel, to define correlations across the input space (such as process parameters) and generate a distribution of likely curves. These curves are compiled into a probabilistic prediction of both the underlying trend and the associated uncertainty, consistent with the noisy and limited test data.

The data analyzed in this work consists of LSS obtained from the ultrasonic welding process development effort for the weldability study with the TC1225 material system (16-ply QI adherends). A design of experiments (DOE) was used to generate the GPR input space by varying three key process parameters: speed, force, and amplitude. Two samples were fabricated and tested at each DOE point. Sources of uncertainty in this study include variability inherent in the ultrasonic welding process, variability in the LSS measurements, and uncertainty associated with the GPR model predictions.

The GPR framework in this work was constructed using a weighted ensemble approach. Ten GPR models were individually fit to the data using various covariance functions (kernels) and tuned hyperparameters (e.g., length scale, noise parameters). Their predictions were then combined into a composite model. A slice of the composite GPR predictions at a selected amplitude is shown in Figure A.1. The measured LSS values are shown as dots for each speed, while the model's response over interpolated force values is depicted with a dashed line representing the mean and solid lines indicating ±1 standard deviation. Increased uncertainty is evident in regions where duplicate observed data vary widely or data are missing. Note that this slice is part of a larger 3D system, where both the mean and variance incorporate data from adjacent amplitude values not shown here.

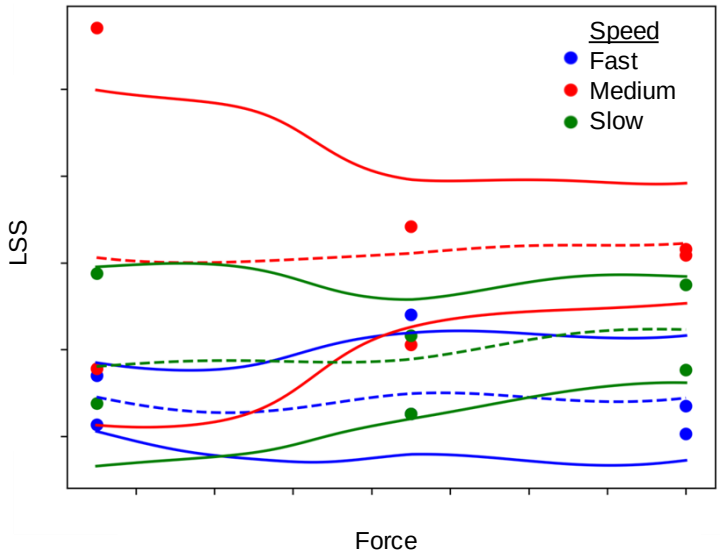


Figure A.1. A slice of ensemble GPR predictions illustrating the SLS mean response and ±1 standard deviation at 60% amplitude.

This analysis indicates that the ultrasonic welding process for LM-PAEK thermoplastic composites is highly variable, but that refinements to the process are likely to increase weld strength and consistency. The GPR model, by effectively filtering noise, identifies trends in the SLS data and highlights regions in the process parameter space where variability is reduced. However, the current test data is limited. To refine these insights and reliably determine an ideal processing window, additional experimental data is needed.